Three-dimensional stress analyses of complex laminated shells with a variable-kinematics continuum shell element

A.K.W. Hii*, S. Minera, R.M.J. Groh, A. Pirrera, L.F. Kawashita

Bristol Composites Institute (ACCIS),
University of Bristol, Queen's Building, University Walk, Bristol, BS8 1TR, UK

Abstract

This paper presents a new variable-kinematics continuum shell (VKCS) element that can be used to model laminated shell structures with arbitrary geometry in a finite element (FE) setting. The novelty is in the implementation of variable-kinematics capability in a continuum shell formulation, using Carrera's Unified Formulation (CUF). The resultant model has completely general geometric and kinematic descriptions. In the formulation, the geometrical representation is based on a numerical isoparametric map with no simplifying assumptions on the shell geometry; whereas the element displacement fields are written in terms of the Fundamental Nuclei according to CUF. In the variable-kinematics framework, the levels of *hp*- and *p*- refinements in the through-thickness and in-plane domains are free parameters that can be varied independently. By parametrically varying in-plane mesh densities and model kinematics, model settings with good trade-offs in computational cost and desired level of accuracy can be identified. In addition to the existing literature benchmarks, we include new 3D stress benchmarks for laminated shells with complex geometrical features, such as spatially varying curvatures, non-orthogonal coordinate lines and variable thicknesses. The higher-order models yield asymptotically correct three-dimensional stresses, even in regions near singularities, without requiring numerical artefacts nor stress recovery procedures. In terms of computational efficiency, the model variants utilising high *p*- level require fewer total degrees of freedom (dofs) compared with linear 3D finite element method (FEM) for convergence of the 3D stress field. In terms of wider applications, the compact formulation can allow for the same computer code and model mesh to be used across a wide range of analyses for complex shell structures that requires different model fidelity, with minimal inputs from the user.

Keywords: Continuum shell finite element, 3D stress fields, Carrera's Unified Formulation, laminated shell structures

1. Introduction

1.1. Background

Due to their efficiency at supporting loads, curved shell structures are often used in engineering application. The popularity of displacement-based shell finite elements (with Kirchhoff or

*Corresponding author.
Email address: aewis.hii@bristol.ac.uk (A.K.W. Hii)

Reissner-Mindlin assumptions) in the analysis of thin-walled structures is attributed to their low computation cost; intuitive and easily applied displacement boundary conditions; and asymptotic convergence of the displacements fields. Together with artefacts such as shear correction factors, reduced integration technique, assumed strains and hourglass controls, displacement-based shell finite elements make up a large proportion of the shell element libraries in commercial finite element codes.

In most thin-walled applications, metallic shell structures exhibit negligible deformation through-thickness. This assumption was explicitly incorporated in the early shell models [1–3], where researchers neglected the strain energy contribution from through-thickness deformation. Shell models can be categorised into models with different through-thickness kinematic assumptions, namely equivalent single layer (ESL) and layer-wise (LW) theories. In ESL models, the heterogenous layup is made statically equivalent to that of a single layer, with a global stiffness that is a weighted average of all the layers. Historically, distortions in the thickness direction are accounted for through the application of shear correction factors, in first order shear deformation theories [4–6]; or via higher-order shear deformation shell theories [7–9]. The shear correction approach is not generally preferred as it involves ad-hoc corrections to the transverse shear strain energy and does not capture higher-order variations through the thickness. On the other hand, higher-order shear deformable shell theories found their way into many shell models such as the 6-parameter [10, 11], 7-parameter [12–14] and 12-parameter [15] formulations. The general trend is that the model accuracy improves with the number of physically meaningful terms in the description of the displacement fields. For models based on LW theories, the displacement fields are treated separately for individual plies or ply blocks, hence providing kinematically accurate transverse shear strains in each material layer [16]. The earlier versions of LW models enforced interlaminar traction continuity by means of constraint equations, such as Lagrange multipliers. Later, Robbins and Reddy [17] showed that the C^0 continuity in the through-thickness displacement, consistent with behaviour of a layered continuum, can naturally be satisfied by using appropriate 1D shape functions based on 1D Lagrange and Legendre polynomials.

In terms of derivations, the shell elements in the literature can be categorised into those developed using different shell theories; or those based on the degenerated 3D elasticity, also known as *continuum shell elements* [18]. Important examples of the former are the theories of the Cosserat brothers [19], Koiter [20], Sanders [21] and the geometrically exact stress resultant models by Simo *et al.* [22–25]. Some examples of the latter are Ahmad *et al.* [2], Hughes and Liu [26, 27], Dvorkin and Bathe [28] and Liu *et al.* [29]. In terms of derivation, the two approaches differ only in the reduction of the 3D continuum governing equations, which is generally carried out analytically and numerically in classical shell theory and continuum shell models, respectively. As noted by several authors [23, 30, 31], under the same kinematic assumptions, the two approaches are indeed equivalent. The degenerated 3D elasticity approaches are preferred in present day computational shell analysis as they are better conditioned for numerical implementations, and more readily applied to model complex shell geometries. For a more detailed exposition on the advances of modern day shear deformable plates and shell theories, the reader is referred to Reddy *et al.* [32].

The idea of independent kinematics refinement in the in-plane and through-thickness domains has been explored Düster *et al.* [33] and Actis *et al.* [34]. The former utilised the Legendre polynomials for independent *p*- refinements in the in-plane and through-thickness displacement fields, and demonstrated savings in the overall computational costs. In the latter, a set of hierarchical through-thickness functions are 'optimally-determined' to satisfy 3D equilibrium equations in a weak sense. Both implementations impose some level of coupling between

the in-plane and through-thickness kinematics. On the other hand, Williams proposed unified theoretical frameworks for plate [35, 36] and shell [37] theories to allow for arbitrary through-thickness expansion functions and interfacial constitutive relations. The model expressions are generalised so that any orders of plate/shell theories can be derived from the framework. Furthermore, Carrera [38] established a generalised framework to handle various forms and orders of 1D and 2D theories in a compact manner. The terminology Carrera's Unified Formulation (CUF) was first introduced in 2008 by Demasi [39]. CUF allows for the finite element basis functions and their corresponding axiomatic functions to be defined and refined independently. Hence, users have full control over the type of primary variables and the kinematic fidelity of their models. To date, there are many contributions on finite element models based on the CUF, such as the 3D stress field analyses of complex composite beams [40, 41], plates [42, 43] and shells [44, 45]. They have also been applied to the analysis of shells with complex geometrical features, such as spatially varying curvatures [46, 47] and variable thicknesses [48, 49]. These works have demonstrated the flexibility of CUF at generating different model classes suitable for different applications.

The existing CUF shell formulations belong to the family of finite element models derived from shell theories. The key characteristics of such models are: (i) the Green-Lagrange strain tensors are expressed in terms of quantities of differential geometry, such as principal curvatures and Lamé parameters; (ii) the solution variables, like displacements and rotations are in the principal directions (two principal curvatures and surface normal). CUF shell models utilise a Green-Lagrange strain measure where the coordinate lines are assumed orthogonal. Here, the latter measure is referred to as a reduced strain tensor. When modelling complex shell geometry, the coordinate lines must be carefully defined to compute the strain energy correctly [50]. The reduced strain expressions can be found in early works by Sokolnikoff [51] and Palazzotto [52]. The expressions for the Green-Lagrange strains that consider non-orthogonality in the coordinate lines can be found in Nemeth [53].

Meanwhile, a continuum shell formulation like the Ahmad-Irons-Zienkiewicz element [2] utilises a non-reduced strain tensor, making no assumptions about the shell geometry. The covariant basis vectors and displacement derivatives are directly computed from the isoparametric definitions of the element geometry. The key characteristics of such shell elements are: (i) the formulation does not use principal curvatures nor Lamé parameters; (ii) the dofs are in the directions of the global Cartesian basis. As demonstrated by Büchter and Ramm [30], both continuum shell formulation and the finite element models based on shell theories are energetically equivalent, and differ only in the discretisation scheme.

In this manuscript, we developed a new shell finite element formulation. The novelty is in the derivation of a *continuum shell element* based on CUF, and its applications to model 3D stresses in thick laminated shells with complex geometries. The shell formulation is derived in a curvilinear basis, where the 3D domain of an arbitrary shell element is based on an isoparametric map from a master element to the element midsurface. This is followed by an additional map for the thickness to describe the 3D volume. The advantages of the proposed model are: (i) the displacement fields assumed by the structural element can be refined to any extent, even asymptotically to that of 3D elements; and (ii) arbitrary shell geometries can be modelled, since the geometric mapping is defined numerically. The flexible framework provided by CUF allows various model classes with different in-plane and through-thickness kinematics to be easily generated, hence catering to different types of analyses with a single model. We also present numerical solutions to the 3D stress fields in shell structures with complex geometry, *i.e.* a parabolic hyperboloid shell and a twisted shell with variable thickness. Some considerations in the definition of the ma-

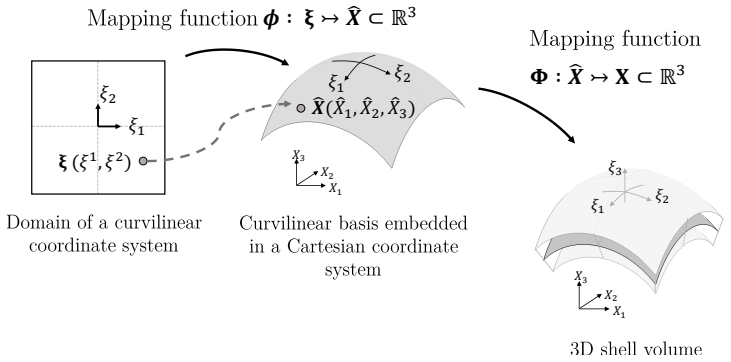

Figure 1: To construct a patch on a surface, a function $\boldsymbol{\phi}: \boldsymbol{\xi} \mapsto \hat{\boldsymbol{X}}$ is used to map the curvilinear coordinates (ξ_1, ξ_2) onto a point $(\hat{X}_1, \hat{X}_2, \hat{X}_3)$ on the patch in the Cartesian basis. Naturally, the curvilinear curves are always tangent to the local surfaces. An additional linear function $\boldsymbol{\Phi}: \hat{\boldsymbol{X}} \mapsto \boldsymbol{X}$ is required to essentially offset the midsurface to produce a shell volume.

terial axes, and the transformation of Cauchy stresses due to the complex geometrical features are also discussed in this article.

1.2. Paper outline

In Section 2.1, we apply the concepts of differential geometry to describe the geometry and kinematics of a continuum in the curvilinear bases. In Section 2.2, we describe the constitutive relations in terms of strain and stress conjugates, along with the definitions of some necessary basis transformations. In Section 2.3, we apply variational principles to derive the governing mathematical expressions for the physical system. Then, in Section 3, we discretise all the governing equations to be solved with the Finite Element Method. In Section 4, we introduce CUF into FEM, along with examples of its application in constructing different types of shell models. In Section 6, we provide some numerical benchmarks to the model. Concluding remarks are presented in Section 7.

2. Governing equations

2.1. Geometric and kinematic description of a continuum

Mathematically, a shell is a 3D object embedded in a 3D Euclidean space. We construct the 3D volume from a 2D surface embedded in the same space using a curvilinear system. In differential geometry, a surface is a combination of patches (or local surfaces) [54], which are defined as vector-valued functions of two curvilinear coordinates ξ_1 and ξ_2, where $\boldsymbol{\xi} = [\xi_1, \xi_2]$. The mapping of a patch is illustrated in Fig. 1. It is written as $\boldsymbol{\phi}: \boldsymbol{\xi} \mapsto \hat{\mathbf{X}}$, where $\boldsymbol{\phi}$ is always differentiable and $\mathbf{X} = [\hat{X}_1, \hat{X}_2, \hat{X}_3]$ is the position vector of a point on the surface in the Cartesian coordinate system. To extend the 2D surface to a 3D continuum, a linear map $\boldsymbol{\Phi}: \hat{\mathbf{X}} \mapsto \mathbf{X}$ along the normal direction of the shell is required, where $\mathbf{X}$ is the position occupied by a point in the shell volume. The mappings can be established analytically or more often numerically.

At any point in the shell volume, we can arbitrarily define a pair of *linearly dependent* tangent vectors as

$$\mathbf{G}_i = \frac{\partial \mathbf{X}}{\partial \xi_\alpha} \quad \text{where} \quad \alpha = 1, 2. \tag{1}$$

Note that $\mathbf{G}_1$ and $\mathbf{G}_2$ are orthogonal and conjugate for some geometries, such as spherical, cylindrical, or any surfaces of revolution. The tangent vectors are also known as the covariant basis vectors—upon a change in basis, the new components of the tangent vectors are linear combinations of the old components. An additional covariant basis vector is defined as

$$\mathbf{G}_3 = \frac{\partial \mathbf{X}}{\partial \xi_3}, \tag{2}$$

where ξ_3 corresponds to the curvilinear coordinates in the shell thickness direction. Naturally, the direction of $\mathbf{G}_3$ aligns with the normal to the local surface. The three covariant basis vectors are now used to define the differential volume of a continuum. A differential line is written as:

$$\mathrm{d}\mathbf{X} = \mathrm{d}X_1 + \mathrm{d}X_2 + \mathrm{d}X_3 = \mathbf{G}_1\,\mathrm{d}\xi_1 + \mathbf{G}_2\,\mathrm{d}\xi_2 + \mathbf{G}_3\,\mathrm{d}\xi_3\,. \tag{3}$$

By combining Eq. (1) and (2), we re-write Eq. (3) in the matrix form as:

$$\begin{Bmatrix} \mathrm{d}X_1 \\ \mathrm{d}X_2 \\ \mathrm{d}X_3 \end{Bmatrix}^\top = \begin{Bmatrix} \mathrm{d}\xi_1 \\ \mathrm{d}\xi_2 \\ \mathrm{d}\xi_3 \end{Bmatrix}^\top \begin{bmatrix} \frac{\partial X_1}{\partial \xi_1} & \frac{\partial X_2}{\partial \xi_1} & \frac{\partial X_3}{\partial \xi_1} \\ \frac{\partial X_1}{\partial \xi_2} & \frac{\partial X_2}{\partial \xi_2} & \frac{\partial X_3}{\partial \xi_2} \\ \frac{\partial X_1}{\partial \xi_3} & \frac{\partial X_2}{\partial \xi_3} & \frac{\partial X_3}{\partial \xi_3} \end{bmatrix} = \begin{Bmatrix} \mathrm{d}\xi_1 \\ \mathrm{d}\xi_2 \\ \mathrm{d}\xi_3 \end{Bmatrix}^\top [\mathbf{J}], \tag{4}$$

where $\mathbf{J}$ is the Jacobian matrix, also known as the Cartesian transformation tensor matrix. Its determinant J corresponds to the differential volume.

The deformation process of a continuum is described via a mapping $\boldsymbol{\chi} : \mathbf{X} \mapsto \mathbf{x}$, where $\mathbf{x}$ is the position vector in the deformed configuration. Its displacements are defined as the difference between the position vectors in the deformed and un-deformed configurations, *i.e.* $\mathbf{u} = \mathbf{x} - \mathbf{X}$.

2.2. Constitutive relations

The proposed formulation is geometrically linear. Both displacements and strains are assumed as infinitesimal during the deformation process. A suitable *small* strain measure is the *linear* part of the Green-Lagrange strain tensor, defined as

$$E_{ij} = \frac{1}{2}\left(\mathbf{G}_i \cdot \mathbf{u}_{,j} + \mathbf{G}_j \cdot \mathbf{u}_{,i}\right) \quad \text{where} \quad i, j = 1, 2, 3, \tag{5}$$

where the comma indicates a partial differential operation. The energy conjugate to the small strain measure is the *Cauchy* stress tensor, denoted as σ Assuming a Cauchy linear-elastic material model, a Saint-Venant Kirchhoff-type material law can be applied. In the absence of stress prior to load application, σ and $\mathbf{E}$ follow Hooke's law:

$$\boldsymbol{\sigma} = \mathbf{C} : \mathbf{E}, \tag{6}$$

where $\mathbf{C}$ is the material tensor. The stress and strain tensors are written as six-part vectors using the Voigt-Kelvin notation:

$$\mathbf{E}^\top = \{E_{11}, E_{22}, E_{33}, E_{23}, E_{13}, E_{12}\}^\top, \tag{7}$$

$$\boldsymbol{\sigma}^{\top} = \{\sigma_{11}, \sigma_{22}, \sigma_{33}, \sigma_{23}, \sigma_{13}, \sigma_{12}\}^{\top}. \tag{8}$$

In a general curvilinear coordinate system, any tensorial quantity is expressed with respect to their covariant or contravariant bases. For energetic conjugacy, this means that the Green-Lagrange strain is written in the covariant basis, as per Eq. (5); and the Cauchy stress in the contravariant basis. Adopting the Einstein notation, Eq. (6) becomes

$$\sigma^{ij} = C^{ijkl} E_{kl}, \quad \text{with} \quad i, j, k, l = 1, 2, 3, \tag{9}$$

where C^{ijkl} is the contravariant form of the material tensor $\mathbf{C}$. The covariant form of the material tensor is denoted as C_{ijkl} in Einstein notation, and $\mathbb{C}$ in the matrix form. We also assume the symmetry of material tensor follows $C_{ijkl} = C_{klij} = C_{jikl} = C_{ijlk} = C_{jilk}$ [55]. The contravariant transformation of C_{ijkl} requires the definition of a set of *orthonormal* local material axes for every material point. For fibrous composites shells, we take $\hat{\mathbf{e}}_1$, $\hat{\mathbf{e}}_2$, and $\hat{\mathbf{e}}_3$ as the fibre, matrix and normal directions respectively. In a general shell structure, we adopt the methodology from Dvorkin *et al.* [28] to construct the material axes as

$$\begin{aligned} \hat{\mathbf{e}}_1 &= \frac{\mathbf{G}_1}{|\mathbf{G}_1|}, \\ \hat{\mathbf{e}}_3 &= \frac{\mathbf{G}_1 \times \mathbf{G}_2}{|\mathbf{G}_1 \times \mathbf{G}_2|}, \\ \hat{\mathbf{e}}_2 &= \frac{\hat{\mathbf{e}}_1 \times \hat{\mathbf{e}}_3}{|\hat{\mathbf{e}}_1 \times \hat{\mathbf{e}}_3|}. \end{aligned} \tag{10}$$

This definition implies that the 0° fibre path aligns with the ξ_1 coordinate curves, and the material normals coincide with the local midsurface normals. For angled plies, we use the definitions of material axes in Eq. (10) along with a transformed $\mathbf{C}$ matrix according to the local ply angle [18]. We note that it is also possible to avoid doing angular transformation to the $\mathbf{C}$ matrix, and instead build the material axes such that $\hat{\mathbf{e}}_1$ and $\hat{\mathbf{e}}_2$ directly align with the angled fibre and matrix directions respectively [14, 15].

Although it is always possible to numerically define the fibre paths and layups on complex surfaces, they may not be achievable from a manufacturing point of view. This is especially the case for shells whose coordinate curves ξ_1 and ξ_2 are non-orthogonal nor conjugate. Taking a cross ply (0°/90°) saddle shell for example, it is challenging to enforce the orthogonality between the two layers globally without excessive shearing of the plies or tows (which results in a non-uniform distribution of volume fraction).

The material tensor in the contravariant form is obtained using basis transformation rules for a rank-4 tensor. Following the Voigt-Kelvin conventions defined in Eq. (7) and (8), the transformation matrix is written as

$$\mathbf{Q} = \begin{bmatrix} l_1^2 & m_1^2 & n_1^2 & m_1 n_1 & n_1 l_1 & l_1 m_1 \\ l_2^2 & m_2^2 & n_2^2 & m_2 n_2 & n_2 l_2 & l_2 m_2 \\ l_3^2 & m_3^2 & n_3^2 & m_3 n_3 & n_3 l_3 & l_3 m_3 \\ 2l_2 l_3 & 2m_2 m_3 & 2n_2 n_3 & m_2 n_3 + m_3 n_2 & n_2 l_3 + n_3 l_2 & l_2 m_3 + l_3 m_2 \\ 2l_3 l_1 & 2m_3 m_1 & 2n_3 n_1 & m_3 n_1 + m_1 n_3 & n_3 l_1 + n_1 l_3 & l_3 m_1 + l_1 m_3 \\ 2l_1 l_2 & 2m_1 m_2 & 2n_1 n_2 & m_1 n_2 + m_2 n_1 & n_1 l_2 + n_2 l_1 & l_1 m_2 + l_2 m_1 \end{bmatrix}, \tag{11}$$

where $l_i = \mathbf{G}^1 \cdot \hat{\mathbf{e}}_i$, $m_i = \mathbf{G}^2 \cdot \hat{\mathbf{e}}_i$, $n_i = \mathbf{G}^3 \cdot \hat{\mathbf{e}}_i$ and $\mathbf{G}^i$ are the contravariant basis vectors. To compute these, we first define the covariant metric tensor as $G_{ij} = G_i\, G_j$. The contravariant metric tensor is the inverse of the covariant metric tensor $G^{ij} = (G_{ij})^{-1}$. Subsequently, the contravariant basis vectors are computed as $G^i = G^{ij} G_j$. The contravariant transformation of the material tensor is

$$\mathbb{C} = \mathbf{Q}^\top \mathbf{C}\, \mathbf{Q}. \tag{12}$$

2.3. Principle of Virtual Work

Similar to most physical systems, the mathematical expressions approximating the elastic behaviour of a shell body is obtained via the application of the calculus of variations to a functional. In solid mechanics, the chosen functional is often the strain energy of the body, a scalar quantity invariant to any admissible basis. This subset to the variational principles is also known as the Principle of Virtual Work (PVW). By neglecting the inertial forces in the linear momentum balance equations, the problem is reduced to a static one. Equilibrium requires that the sum of variations in the internal and external strain energy to be null, or at least to a sufficiently low residual [56, 57],

$$\delta\Pi_{\text{int}} - \delta\Pi_{\text{ext}} = 0, \tag{13}$$

where δ denotes the variational operator, and Π_{int} and Π_{ext} are the strain energy due to the elastic deformation and externally applied loads, respectively. Henceforth, they are known as the internal and external strain energy respectively. The internal strain energy variation is defined as:

$$\delta\Pi_{\text{int}} = \int \boldsymbol{\sigma} : \delta\mathbf{E}\, \mathrm{d}\mathcal{B}\,, \tag{14}$$

where $\mathcal{B}$ denotes the continuum volume, $\boldsymbol{\sigma}$ and $\mathbf{E}$ are the *Cauchy* stress tensor and the *Green-Lagrange* strain tensor respectively as defined in Section 2.2. The variation of the external work done is written as:

$$\delta\Pi_{\text{ext}} = -\int \mathbf{b} \cdot \delta\mathbf{u}\, \mathrm{d}\mathcal{B} - \int \hat{\mathbf{t}} \cdot \delta\mathbf{u}\, \mathrm{d}\Gamma\,, \tag{15}$$

where $\mathbf{b}$ is the body force, $\hat{\mathbf{t}}$ is the traction on the boundaries, $\delta\mathbf{u}$ is the virtual variation of displacements and the domain Γ denotes the boundary of a continuum.

3. Discretisation with the Finite Element Method

In previous sections, the general governing equations to model the infinitesimal deformation of a shell body are introduced. We adopt the Finite Element Method to approximate the solution to the equations. In this section, we present the discretisation of the shell geometry and strain energy expressions.

3.1. Discretisation of geometry

The geometric discretisation of the shell body begins with the creation of a midsurface. Patches on the midsurface are represented by a finite element, and constructed by element-wise interpolation of the finite element nodal coordinates. Following the discretisation technique in [14, 28, 58, 59], the position vector on the midsurface $\hat{\mathbf{X}}$ is written as:

$$\hat{\mathbf{X}} = N_k(\xi_1, \xi_2)\, \hat{\mathbf{X}}_k \quad \text{where } (\xi_1, \xi_2) \in \Omega^{(e)}, \tag{16}$$

where k corresponds to the k-th node in a finite element, N_k are any admissible 2D interpolation functions, $\hat{\mathbf{X}}_k$ are the coordinates of the midsurface nodes, $\Omega^{(e)}$ denotes the element area and the superscript (e) indexes the finite element. Upon discretisation of a geometry in FEM, it is convenient to set the curvilinear coordinates $\boldsymbol{\xi}$, as discussed in Section 2.1, to be the same as the coordinates of a master finite element. In doing so, it is straightforward to compute the tangent vectors, where only the finite element nodal coordinates and the shape functions are required. The 3D volume is constructed via the linear map $\boldsymbol{\Phi} : \hat{\mathbf{X}} \mapsto \mathbf{X}$ as

$$\mathbf{X} = \hat{\mathbf{X}} + \frac{h_k(\xi_1, \xi_2)}{2}\, \xi_3\, N_k(\xi_1, \xi_2)\, \hat{\mathbf{D}}_k, \tag{17}$$

where $\hat{\mathbf{D}}_k$ are the unit normals (also known as the *directors*) at the FE nodes. The discretised covariant basis vectors from Eq. (1) and (2) read:

$$\begin{aligned} \mathbf{G}_\alpha = \mathbf{X}_{,\alpha} &\equiv \frac{\partial \mathbf{X}}{\partial \xi_\alpha}, \quad \alpha = 1, 2 \\ &= \frac{\partial}{\partial \xi_\alpha}(N_k\, \hat{\mathbf{X}}_k + \frac{h_k}{2}\, \xi_3 N_k\, \hat{\mathbf{D}}_k) \\ &= \frac{\partial N_k}{\partial \xi_\alpha}(\, \hat{\mathbf{X}}_k + \frac{h_k}{2}\, \xi_3\, \hat{\mathbf{D}}_k), \end{aligned} \tag{18}$$

where the comma indicates a partial differential operation. Similarly, the covariant basis vector corresponding to the shell through-thickness direction is

$$\begin{aligned} \mathbf{G}_3 = \mathbf{X}_{,3} &\equiv \frac{\partial \mathbf{X}}{\partial \xi_3} \\ &= \frac{h_k}{2}\, N_k\, \hat{\mathbf{D}}_k. \end{aligned} \tag{19}$$

3.2. Discretisation of the strain energy variation

In FEM, we postulate that variation of the energy functional in a system is the sum of all its element-wise variations, hence

$$\delta\Pi_{\text{int}} = \sum_e^{N_e} \delta\Pi_{\text{int}}^{(e)} \quad \text{and} \quad \delta\Pi_{\text{ext}} = \sum_e^{N_e} \delta\Pi_{\text{ext}}^{(e)}, \tag{20}$$

where N_e denotes the number of elements in the FE domain, and the superscript $(\cdot)^{(e)}$ is the element index. The finite element method satisfies the equilibrium equations only in a weak sense, as the equilibrium is only enforced in an integral sense across the finite element domain.

The external strain energy manifests as an energy contribution from different loading conditions. Indices $i, j = 1, ..., n$ refer to the finite element nodes, where n denotes the number of nodes in an element. In particular, nodal index j denotes variation of primary variables, and Eq. (15) is re-written as

$$-\delta\Pi_{\text{ext}}^{(e)} = \delta\mathbf{u}_j^\top \mathbf{f}^{(e)}, \tag{21}$$

where j indexes the displacements at the FE nodes and $\mathbf{f}^{(e)}$ denotes the equivalent nodal force vector corresponding to all the loading conditions. Readers are referred to Ref. [60] for a detailed

explanation on the computation of $\mathbf{f}^{(e)}$ for different loading conditions. By discretising Eq. (14), we write the internal strain energy as

$$\begin{aligned}\delta\Pi_{\text{int}}^{(e)} &= \int \delta\mathbf{E}^{\top}\ \boldsymbol{\sigma}\ \mathrm{d}\mathcal{B}^{(e)} \\ &= \delta\mathbf{u}_j^{\top} \int \mathbf{B}^{\top}\mathbf{C}\,\mathbf{B}\ \mathrm{d}\mathcal{B}^{(e)}\,\mathbf{u}_i \\ &= \delta\mathbf{u}_j^{\top}\,\mathbf{k}^{(e)}\,\mathbf{u}_i,\end{aligned}$$

where i indexes the primary variables at the FE nodes, $\mathbf{k}^{(e)}$ is the stiffness matrix corresponding to each finite element, $\mathbf{B}$ is the shape function differential matrix and $d\mathcal{B}^e$ is the differential element volume. Conventionally, $\mathbf{B}$ is defined as

$$\mathbf{B} = \mathcal{D}\mathcal{N}, \tag{22}$$

where $\mathcal{D}$ is a differential operator corresponding to the definition of $\mathbf{E}$, and $\mathcal{N}$ is any admissible set of three-dimensional interpolation functions for the kinematics. For simplicity, we re-write the vector components of the covariant base vectors in Eq. (1) and (2) as

$$\begin{Bmatrix}\mathbf{G}_1\\ \mathbf{G}_2\\ \mathbf{G}_3\end{Bmatrix} = \begin{bmatrix}\frac{\partial X_1}{\partial\xi_1} & \frac{\partial X_2}{\partial\xi_1} & \frac{\partial X_3}{\partial\xi_1}\\ \frac{\partial X_1}{\partial\xi_2} & \frac{\partial X_2}{\partial\xi_2} & \frac{\partial X_3}{\partial\xi_2}\\ \frac{\partial X_1}{\partial\xi_3} & \frac{\partial X_2}{\partial\xi_3} & \frac{\partial X_3}{\partial\xi_3}\end{bmatrix} \equiv \begin{bmatrix}X_{1,1} & X_{2,1} & X_{3,1}\\ X_{1,2} & X_{2,2} & X_{3,2}\\ X_{1,3} & X_{2,3} & X_{3,3}\end{bmatrix}. \tag{23}$$

For models in curvilinear coordinate systems, $\mathcal{D}$ corresponds to the linear part of the Green-Lagrange strain tensor and is defined as

$$\mathcal{D} = \begin{bmatrix} X_{1,1}\frac{\partial}{\partial\xi_1} & X_{2,1}\frac{\partial}{\partial\xi_1} & X_{3,1}\frac{\partial}{\partial\xi_1}\\ X_{1,2}\frac{\partial}{\partial\xi_2} & X_{2,2}\frac{\partial}{\partial\xi_2} & X_{3,2}\frac{\partial}{\partial\xi_2}\\ X_{1,3}\frac{\partial}{\partial\xi_3} & X_{2,3}\frac{\partial}{\partial\xi_3} & X_{3,3}\frac{\partial}{\partial\xi_3}\\ X_{1,3}\frac{\partial}{\partial\xi_2} + X_{1,2}\frac{\partial}{\partial\xi_3} & X_{2,3}\frac{\partial}{\partial\xi_2} + X_{2,2}\frac{\partial}{\partial\xi_3} & X_{3,3}\frac{\partial}{\partial\xi_2} + X_{3,2}\frac{\partial}{\partial\xi_3}\\ X_{1,3}\frac{\partial}{\partial\xi_1} + X_{1,1}\frac{\partial}{\partial\xi_3} & X_{2,3}\frac{\partial}{\partial\xi_1} + X_{2,1}\frac{\partial}{\partial\xi_3} & X_{3,3}\frac{\partial}{\partial\xi_1} + X_{3,1}\frac{\partial}{\partial\xi_3}\\ X_{1,2}\frac{\partial}{\partial\xi_1} + X_{1,1}\frac{\partial}{\partial\xi_2} & X_{2,2}\frac{\partial}{\partial\xi_1} + X_{2,1}\frac{\partial}{\partial\xi_2} & X_{3,2}\frac{\partial}{\partial\xi_1} + X_{3,1}\frac{\partial}{\partial\xi_2} \end{bmatrix}. \tag{24}$$

4. Finite Element Method with Carrera's Unified Formulation

In this section, we introduce the notations from CUF into the strain energy variation and yield a variable-kinematics continuum shell formulation in a curvilinear system. Conventional FE formulations and the CUF share the same energy functional and variations. In the latter, the element-wise stiffness matrices are assembled from sub-blocks of *Fundamental Nuclei* (FN), which are dofs at the sub-element level. To demonstrate the concept of dofs at the sub-element level, we will draw an equivalence between a displacement-based 8-noded solid element and its shell counterpart: in the former, all the dofs are directly interpreted at the FE nodes. Its shell counterpart consists of a 2D element with four nodes, paired with a two-noded one dimensional

thickness function. The dofs at the 'sub-element' level are therefore the displacements at the top and bottom surface of the shell.

The stiffness matrix of any 1D or 2D model derived from CUF is assembled with respect to four indices i, j, τ, s. The indices i and j denote dofs at the FE node level and their variations, respectively. On the other hand, τ and s denote the sub-element dofs and their variations, respectively. For more backgrounds on CUF, readers are referred to Ref. [61]. Although there are no restrictions to the type of dofs that are admissible in the axiomatic expansion functions, in most cases they are defined as displacements at specific locations, or rotations about the midsurface FE nodes.

CUF allows free axiomatic expansion of primary variables in structural theories. In the case of 2D shell theories, the displacement fields $\mathbf{u}(\xi_1, \xi_2, \xi_3)$ and their virtual variations can be interpolated by means of independently defined in-plane and thickness functions, indexed by (i, j, τ, s), as

$$\mathbf{u}(\xi_1, \xi_2, \xi_3) = F_\tau(\xi_3)\, N_i(\xi_1, \xi_2)\, \mathbf{u}_{\tau i} \quad \text{with} \quad \tau = 1, ..., m \quad \text{and} \quad i = 1, ..., n, \tag{25}$$

$$\delta\mathbf{u}(\xi_1, \xi_2, \xi_3) = F_s(\xi_3)\, N_j(\xi_1, \xi_2)\, \delta\mathbf{u}_{sj} \quad \text{with} \quad s = 1, ..., m \quad \text{and} \quad j = 1, ..., n, \tag{26}$$

where $F_{(\cdot)}$ are the thickness functions, $N_{(\cdot)}$ are the in-plane interpolating functions, m is the number of terms in the axiomatic expansion, and n is the number of terms in the in-plane functions. In terms of 2D models, the implementations of different orders/types of higher-order shear, layerwise and zig-zag theories in CUF differ only in the choice of thickness functions [62].

The models derived via CUF are 3D in nature, as no simplifying assumptions are made regarding the kinematics of a continuum. In a typical 2D formulation, as in the vast number of shell models in the literature, dimensional reduction is conducted in the sense that the through-thickness strains (normal stretching and transverse shear) are zeroed. Since the same $F_{(\cdot)}$ is applied to all the strain components, omission of any strain components have to be enforced after the stiffness matrix is assembled. To achieve dimensional reduction directly with CUF, readers are referred to Demasi's work [63] on the Generalised Unified Formulation (GUF), where their expressions allow all the strain components to be interpolated with different axiomatic functions.

Here, we demonstrate the application of CUF to derive different types of shell models. The displacement fields of an ESL shell model with an arbitrary order of through-thickness shear and normal deformation can be written as

$$\begin{aligned} \mathbf{u}_i(\xi_1, \xi_2, \xi_3) &= F_1\mathbf{u}_{1i} + F_2\mathbf{u}_{2i} + F_3\mathbf{u}_{3i} + ...F_m\mathbf{u}_{mi}, \quad i = 1, ..., n, \\ F_1 &= \left(\xi_3 \frac{h}{2}\right), \quad F_2 = \left(\xi_3 \frac{h}{2}\right)^2, \quad ..., \quad F_m = \left(\xi_3 \frac{h}{2}\right)^m, \end{aligned} \tag{27}$$

where i indexes the finite element nodes, $F_{(\cdot)}$ is a thickness function similar to a Taylor series expansion. Cinefra *et al.* [64] showed that thickness functions based on trigonometric sine, cosine and exponential series are also admissible to model higher-order shear deformation theories. As a second example, a displacement field based on a layer-wise approach can read

$$\mathbf{u}_i^p(\xi_1, \xi_2, \xi_3) = F_t^p\mathbf{u}_{ti}^p + F_b^p\mathbf{u}_{bi}^p + F_{r_1}^p\mathbf{u}_{r_1 i}^p + F_{r_2}^p\mathbf{u}_{r_2 i}^p + ... + F_{r_m}^p\mathbf{u}_{r_m i}^p, \quad i = 1, ..., n, \tag{28}$$

where $F_{(\cdot)}^p$ are the coefficients of piecewise functions such as Lagrange and Legendre polynomials, superscript p indexes the material layer, subscripts t denotes top surface, b denotes bottom surface, and r_i denotes the polynomial terms. In this approach, the kinematics in every shell layer is explicitly described, and the continuity conditions at the layer interfaces are enforced via

assembly of 1D polynomials with C^0 displacement continuity at the nodes, or some constraint equations [17, 65].

Having written the displacement fields in terms of CUF, the strain energy expressions are ready to be discretised. We re-write Eq. (22) as

$$\begin{aligned}\delta\Pi_{\text{int}}^{(e)} &= \delta\mathbf{u}_{sj}\int \mathbf{B}^{\top}\mathbf{C}\,\mathbf{B}\;\mathrm{d}\mathcal{B}^{(e)}\;\;\mathbf{u}_{\tau i}\\ &= \delta\mathbf{u}_{js}^{\top}\mathbf{k}_{ij\tau s}^{(e)}\mathbf{u}_{\tau i},\end{aligned} \tag{29}$$

where $\mathbf{k}_{ij\tau s}$ is the FN of an element-wise stiffness matrix. The advantage of writing the stiffness matrix this way is that the stiffness components corresponding to a degree of freedom of interest can easily be identified using the four indices. The expression for external energy is shown here for completeness

$$-\delta\Pi_{\text{ext}}^{(e)} = \delta\mathbf{u}_{js}^{\top}\mathbf{f}_{js}^{(e)}. \tag{30}$$

Similar to the global stiffness matrix $\mathbf{K}$, the global load vector $\mathbf{f}$ is an assembly of submatrices of $\mathbf{f}_{js}^{(e)}$. For detailed illustration of the assembly process using the indices i, j, τ, s, readers are referred to Ref. [61].

In a finite element setting, the differentials are approximated via derivatives of the interpolating functions. Using expressions of displacement fields from Eq. (25) and (26), the differentials of the 3D interpolation functions $\boldsymbol{\mathcal{N}}$ in Eq. (22) are written as

$$\begin{aligned}\frac{\partial\boldsymbol{\mathcal{N}}}{\partial\xi_1} &= \mathbf{F}(\xi_3)\,\frac{\partial\mathbf{N}(\xi_1,\xi_2)}{\partial\xi_1} \equiv \mathbf{F}(\xi_3)\,\mathbf{N}_{,1}(\xi_1,\xi_2),\\ \frac{\partial\boldsymbol{\mathcal{N}}}{\partial\xi_2} &= \mathbf{F}(\xi_3)\,\frac{\partial\mathbf{N}(\xi_1,\xi_2)}{\partial\xi_2} \equiv \mathbf{F}(\xi_3)\,\mathbf{N}_{,2}(\xi_1,\xi_2),\\ \frac{\partial\boldsymbol{\mathcal{N}}}{\partial\xi_3} &= \frac{\partial\mathbf{F}(\xi_3)}{\partial\xi_3}\,\mathbf{N}(\xi_1,\xi_2) \equiv \mathbf{F}_{,3}(\xi_3)\,\mathbf{N}(\xi_1,\xi_2).\end{aligned} \tag{31}$$

By combining Eq. (22), (24) and (31), we can write the shape function differentials as

$$\mathbf{B} = \begin{bmatrix} X_{1,1}F_\tau N_{i,1} & X_{2,1}F_\tau N_{i,1} & X_{3,1}F_\tau N_{i,1}\\ X_{1,2}F_\tau N_{i,2} & X_{2,2}F_\tau N_{i,2} & X_{3,2}F_\tau N_{i,2}\\ X_{1,3}F_{\tau,3}\,N_i & X_{2,3}F_{\tau,3}\,N_i & X_{3,3}F_{\tau,3}\,N_i\\ X_{1,3}F_\tau N_{i,2} + X_{1,2}F_{\tau,3}\,N_i & X_{2,3}F_\tau N_{i,2} + X_{2,2}F_{\tau,3}\,N_i & X_{3,3}F_\tau N_{i,1} + X_{3,2}F_{\tau,3}\,N_i\\ X_{1,3}F_\tau N_{i,1} + X_{1,1}F_{\tau,3}\,N_i & X_{2,3}F_\tau N_{i,1} + X_{2,1}F_{\tau,3}\,N_i & X_{3,3}F_\tau N_{i,1} + X_{3,1}F_{\tau,3}\,N_i\\ X_{1,2}F_\tau N_{i,1} + X_{1,1}F_\tau N_{i,2} & X_{2,2}F_\tau N_{i,1} + X_{2,1}F_\tau N_{i,2} & X_{3,2}F_\tau N_{i,1} + X_{3,1}F_\tau N_{i,2}\end{bmatrix}. \tag{32}$$

Note that the $\mathbf{B}$ corresponding to the virtual variations is obtained by simply substituting indices (τ, i) with (s, j) in Eq. (32). The fundamental nuclei is expressed as

$$\underset{(\mathrm{N_{var}}\times\mathrm{N_{var}})}{\mathbf{k}_{ij\tau s}^{(e)}} = \int \underset{(\mathrm{N_{var}}\times 6)}{\mathbf{B}^{\top}}\;\;\underset{(6\times 6)}{\mathbf{C}}\;\;\underset{(6\times\mathrm{N_{var}})}{\mathbf{B}}\;\mathrm{d}\mathcal{B}^{(e)}, \tag{33}$$

where $\mathrm{N_{var}}$ is the number of *components* in the generalised displacement vector. Since we are interested in the displacements in the 3D space only, typically $\mathrm{N_{var}} = 3$, which indicates displacements about the (X_1, X_2, X_3) coordinates. Since the global stiffness matrix $\mathbf{K}$ is simply an assembly of the FN in all the elements, the form and order of the expansion functions can easily

be changed. For the definitions of FNs for multi-field analyses, readers are referred to Ref. [66]. In Eq. (33), we have established the FN of the variable-kinematics continuum shell element. The explicit expressions of the FN are rather intricate, and the resultant expressions for the nine components of $\mathbf{k}^{(e)}_{ij\tau s}$ are provided in Appendix A.

For completeness, the global solution vector for the generalised displacement is $\mathbf{U}$, obtained using standard finite element procedure as

$$\mathbf{KU} = \mathbf{f}. \tag{34}$$

5. Hierarchical basis functions

In our implementation, the planar and through-thickness basis functions consist of the Lagrange polynomials. The basis functions and their differentials can be recursively generated in a straightforward manner, which is beneficial in the implementation of a variable-kinematics model. Unlike most shell models that have displacements and rotations dofs [3, 14, 15, 34], our implementation of VKCS only has displacements dofs as a result of the choice of planar and through-thickness basis functions. The resultant shell model is conceptually similar to a solid-shell, where no rotational dofs are involved. The use of Lagrange polynomials in describing the through-thickness kinematics is beneficial, they are $C^{(n-1)}$ continuous intra-element (where n is the highest polynomial order), and C^0 continuous inter-element. Although the Lagrange polynomials do not directly enforce the interlaminar continuity condition in transverse normal and shear stresses, these properties correspond well to the continuous strains expected within a lamina, and discontinuous transverse shear strains at the ply interfaces.

6. Numerical benchmarks and discussions

In this section, we present three numerical benchmarks to validate the VKCS element, particularly the abilities of the higher-order variants to predict accurate 3D stress fields. In Section 6.1, VKCS is validated with an example taken from the literature. In Section 6.1, we benchmark VKCS against an example taken from the literature. In Section 6.2 and 6.3, VKCS is validated against two new 3D stress benchmarks for geometrically complex shell structures. The reference solutions are obtained via high-fidelity 3D-FEM models in the commercial finite element software Abaqus. The new benchmarks are designed to have doubly curved profiles with non-orthogonal coordinate lines, and exhibit significant through-thickness distortion. In Section 6.3, we conduct a parametric study on model kinematics, to identify models with the best tradeoffs in computational costs and desired level of accuracy. All the VKCS solutions presented are obtained from the layer-wise (LW) models, utilising Lagrange polynomials in the planar and through-thickness basis functions.

6.1. Varadan and Bhaskar's cylinder

Varadan and Bhaskar [67] presented the 3D elasticity solution for a composite cylinder in bending and the resultant three-dimensional stresses. To obtain accurate 3D stress fields, cubic in-plane displacement fields are prescribed to the VKCS model, where the layers are discretised with an assembly of cubic one-dimensional Lagrange polynomials. We performed 3D stress benchmarks on the $(90^\circ/0^\circ/90^\circ)$ laminates with three different R/h ratios, where R and h are radius and thickness respectively. All layers have equal thicknesses. The cylindrical geometry is parameterised via a 2D chart (θ, z), with the model parameters as shown in Table 1.

Table 1: Model parameters for the Varadan and Bhaskar's cylinder numerical benchmark.

Geometry parameterisation:

$$\mathbf{X}(\theta, z) = \begin{bmatrix} R\,\cos(\theta) \\ R\,\sin(\theta) \\ z \end{bmatrix} \quad \textit{where} \;\; 0 \leq \theta \leq 2\pi \text{ and } 0 \leq z \leq L$$

$$R = 1,\; L = 4/R,\; h = [0.25, 0.1, 0.01] \quad \text{such that} \quad R/h = [4, 10, 100]$$

Material properties:

$$E_{11} = 25,\;\; E_{22} = E_{33} = 1,\;\; G_{12} = 0.5,\;\; G_{23} = G_{31} = 0.2,\;\; \nu_{12} = \nu_{13} = \nu_{23} = 0.25$$

$$\text{Layup: } (90^\circ/0^\circ/90^\circ)$$

Material axes:

$$\hat{\mathbf{e}}_1(\theta, z) = \frac{-\sin(\theta)\,\hat{\mathbf{x}}_1 + \cos(\theta)\,\hat{\mathbf{x}}_2}{\| -\sin(\theta)\,\hat{\mathbf{x}}_1 + \cos(\theta)\,\hat{\mathbf{x}}_2 \|}$$

$$\hat{\mathbf{e}}_2(\theta, z) = \hat{\mathbf{x}}_3$$

$$\hat{\mathbf{e}}_3(\theta, z) = \frac{\hat{\mathbf{e}}_1 \times \hat{\mathbf{e}}_2}{\|\hat{\mathbf{e}}_1 \times \hat{\mathbf{e}}_2\|}$$

Loading conditions:

$$\text{Internal sinusoidal pressure } q(\theta, z) = -Q\,\sin(m\pi z/L)\cos(n\theta),$$
$$\text{where } \;\; Q = 1, \;\; m = 1 \;\; \text{and} \;\; n = 4$$

Boundary conditions:

$$\text{Shear diaphragm at } X_3 = 0 \;\; \text{and} \;\; X_3 = L, \;\; \text{where} \;\; u_{\xi_1} = u_{\xi_3} = \sigma_{33} = 0$$

where Q denotes the load amplitude, m and n denote the half waves in the longitudinal and circumferential directions respectively, $\hat{\mathbf{x}}_i$ denotes the global Cartesian unit vectors, the hoop direction $\hat{\mathbf{e}}_1(\theta, z)$ aligns with the fibre direction.

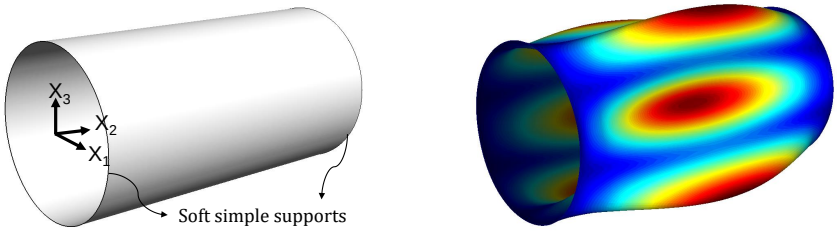

(a) (b)

Figure 2: Un-deformed (a) and deformed configuration (b) of the Varadan & Bhaskar's cylindrical shell benchmark. The boundary conditions are pins with rolling dof in X_2 at $X_2 = [0, L]$. The colour contour refers to the magnitude of displacement.

Shear diaphragm boundary conditions, also known as the soft simple supports are specified at the two ends of the cylinder. The boundary conditions are identical to simply supported edges with translational dofs (rolling pin) in X_2, hence $u_1 = u_3 = 0$ along the midsurface of the cylinder (Fig. 2). The computed 3D stresses are nondimensionalised as below:

$$\begin{aligned}
\bar{\sigma}_{\alpha\alpha} &= \frac{10\,\sigma_{\alpha\alpha}}{Q(R/h)^2}\,[\,\sin(m\pi X_2/L)\cos(n\theta)\,]^{-1}\,,\\
\bar{\sigma}_{33} &= \sigma_{33}\,[\,Q\sin(m\pi X_2/L)\cos(n\theta)\,]^{-1}\,,\\
\bar{\sigma}_{\alpha\beta} &= \frac{10\,\sigma_{\alpha\beta}}{Q(R/h)^2}\,[\,\cos(m\pi X_2/L)\sin(n\theta)\,]^{-1}\,,\\
\bar{\sigma}_{\alpha 3} &= \frac{10\,\sigma_{\alpha 3}}{Q(R/h)}\,[\,\cos(m\pi X_2/L)\cos(n\theta)\,]^{-1}\,,
\end{aligned}$$

where $\alpha, \beta = 1, 2$. The benchmark numerical results in the through-thickness stresses for $R/h = 4, 10$ and 100 are shown in Fig. 3, 4 and 5 respectively. The non-dimensionalised thickness locations are denoted by $\xi_3 \in [-1, 1]$. VKCS-L4 accurately predicts the 3D stresses across the range of R/h ratios. In this case, we prescribe 12 and 15 elements in the hoop and the long directions, respectively, amounting to 56 730 total dofs for convergence in all cases.

6.2. Hyperbolic paraboloid shell

In this section, a challenging benchmark to analyse shells with spatially varying curvatures and non-orthogonal coordinate lines is proposed. The main aim of the benchmark is to showcase the generality and accuracy of the developed VKCS in capturing 3D stresses of an arbitrary smooth surface. The geometry of choice is a deep hyperbolic paraboloid shell, also known as 'hypar' shell, or a saddle. It is a warped surface which can be constructed only by straight lines, and possesses remarkable architectural and mechanical properties. This benchmark presents a challenge for shell formulations whose geometric discretisation and strain measures are expressed in terms of orthogonal principle radii, as this example strongly violates the assumptions of orthogonal and conjugate coordinate lines often made in shell models derived from classical shell theories.

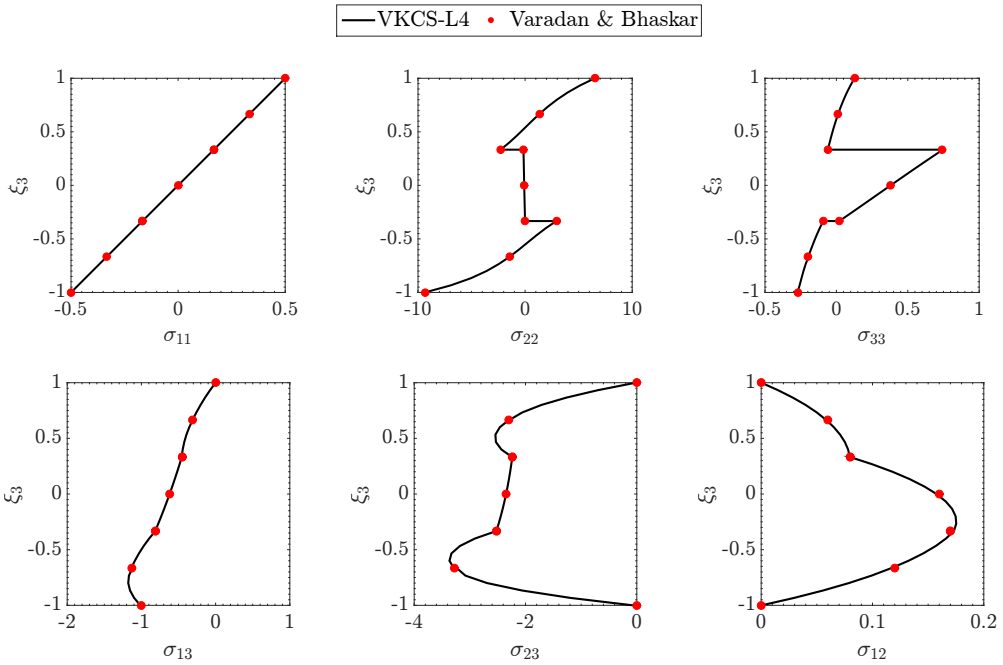

Figure 3: Non-dimensionalised through-thickness stress components of the $R/h = 4$ softly simply supported [90,0,90] Varadan & Bhaskar's cylinder [67] subjected to internal sinusoidal pressure.

There are many studies and mathematical analyses on the behaviour of hypar shells in the literature, with most works reporting their analysis results in terms of spanwise in-plane forces and displacements, such as [68–70]. No through-thickness stress benchmarks have been reported, neither have 3D elasticity solutions been derived for hypar shells. Here, we present a stress benchmark for a hypar shell, whose geometry, loading and boundary conditions can be reproduced easily as an addition to the literature. The hypar shell is thick, deep and consists of 10 cross-plies with equal thickness for all layers, subjected to uniform pressure. The geometry is parameterised with a 2D chart (x, y). To obtain accurate stress fields, we have prescribed kinematics such that the in-plane domain has cubic displacement fields, and each shell layer is again discretised with cubic piecewise Lagrange polynomials. The model parameters are shown in Table 2.

The un-deformed and deformed configurations of the hypar shell midsurface are shown in Fig. 6. The displacement solution along X_1 with $X_2 = 0$ is plotted in Fig. 7, where we observe excellent agreement with 3D-FEM results. The through-thickness stresses of the hypar shell are measured at locations $(x, y) = (0.10, 0.10)$, $(0.48, 0.10)$ and $(0.46, 0.46)$, and the results are shown in Fig. 8, 9 and 10, respectively. The thickness locations are non-dimensionalised as in $\xi_3 \in [-1, 1]$. The latter two locations are sampled at 2% and 4% shell planform length away from the clamped edges, respectively. At $(x, y) = (0.48, 0.10)$, the angle between the coordinate lines is approximately orthogonal, whereas at $(x, y) = (0.46, 0.46)$, the coordinate lines are skewed by more than 40°.

This is a particularly challenging test case, due to the combinations of the following factors: the layup is highly heterogenous; due to the geometry, a structural mesh with good aspect ratio

Table 2: Model parameters for the hypar shell numerical benchmark.

Geometrical parameterisation

$$\mathbf{X}(x,y) = \begin{bmatrix} x \\ y \\ 2(x^2 - y^2) \end{bmatrix} \quad \text{where} \quad -0.5 \leq x \leq 0.5 \quad \text{and} \quad -0.5 \leq y \leq 0.5$$

$$h = 0.075$$

Material properties:

$$E_{11} = 25, \quad E_{22} = E_{33} = 1, \quad G_{12} = 0.5, \quad G_{23} = G_{31} = 0.2, \quad \nu_{12} = \nu_{13} = \nu_{23} = 0.25$$

Layup: $(0^\circ/90^\circ)_5$

Material axes:

$$\hat{\mathbf{e}}_1(x,y) = \frac{\hat{\mathbf{x}}_1 + 4\,x\,\hat{\mathbf{x}}_3}{\|\hat{\mathbf{x}}_1 + 4\,x\,\hat{\mathbf{x}}_3\|}$$
$$\hat{\mathbf{e}}_3(x,y) = \frac{\hat{\mathbf{e}}_1 \times \hat{\mathbf{e}}_2}{\|\hat{\mathbf{e}}_1 \times \hat{\mathbf{e}}_2\|}$$
$$\hat{\mathbf{e}}_2(x,y) = \frac{\hat{\mathbf{e}}_1 \times \hat{\mathbf{e}}_3}{\|\hat{\mathbf{e}}_1 \times \hat{\mathbf{e}}_3\|}$$

Loading conditions:

Uniform pressure on the top surface $q = 1$

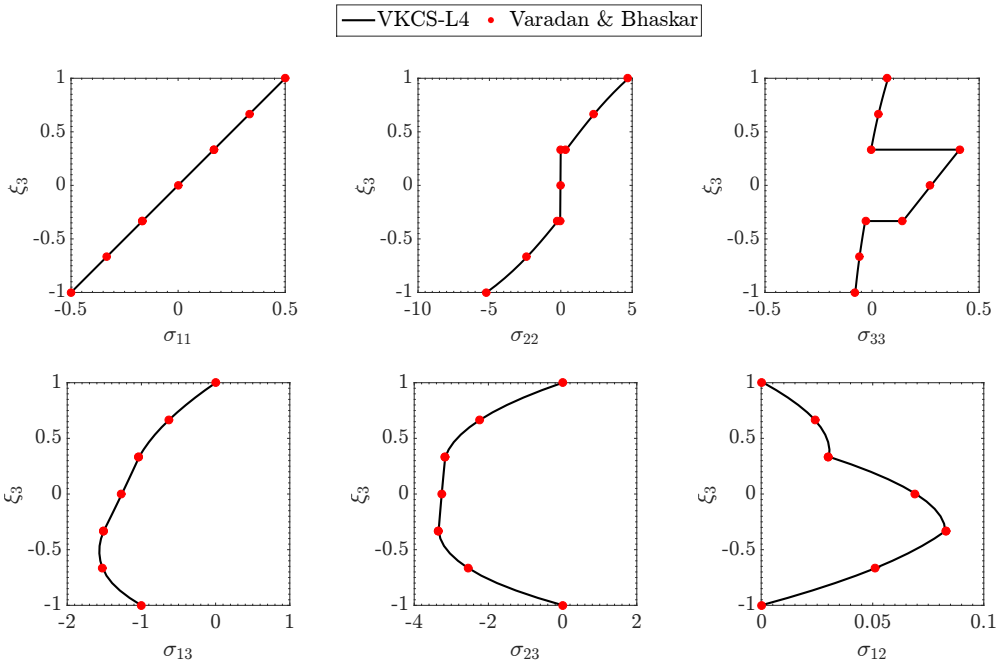

Figure 4: Non-dimensionalised through-thickness stress components of the $R/h = 10$ softly simply supported [90,0,90] Varadan & Bhaskar's cylinder [67] subjected to internal sinusoidal pressure.

elements is not possible, especially near the vertices; and the stresses at the inquired locations are very close to the clamped edges. In our model, we circumvent the potential locking phenomena due to complex element geometry via the use of higher-order in-plane interpolation functions. A total number of 339 915 are required for convergence of stresses in the VKCS model. For convergence in stresses near the vertices, the 3D-FEM model consists of 1 875 000 brick elements with 20 nodes, amounting to 23 200 683 dofs. Numerical results from VKCS shell model remains in excellent agreement with high-fidelity 3D-FEM for this test case across all the locations. Since hypar shells retain the complex surface properties of an arbitrary geometry, we have demonstrated that the VKCS element is well suited to analyse 3D stress fields in complex shell structures.

6.3. Twisted shell with variable thickness

The last benchmark is a twisted laminated shell with variable thickness, as shown in Fig. 11. The geometry is arbitrary and is not based on any specific product. The complex geometrical features of this analytical surface, such as spatial variation in curvatures and thicknesses are commonly found in engineering shell structures, for instance, aircraft engine fan blades and wind turbine blades. To the best of our knowledge, there are no studies in the wider literature that provide three-dimensional stress field benchmarks for shells with these geometrical features. Therefore, sufficient information of the blade geometries, thickness distribution and material axes are provided for interested readers to reproduce the benchmarks.

The definitions of material axes in the in-plane domain must be carefully considered in shells with complex profiles and variable thicknesses. There are two ways to define the material orien-

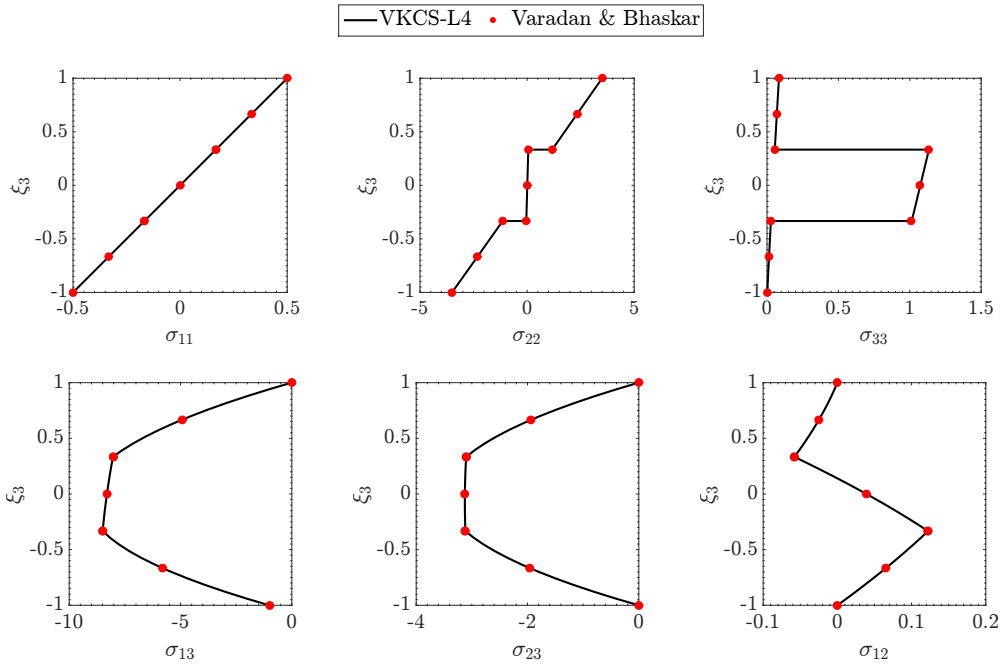

Figure 5: Non-dimensionalised through-thickness stress components of the $R/h = 100$ softly simply supported [90,0,90] Varadan & Bhaskar's cylinder [67] subjected to internal sinusoidal pressure.

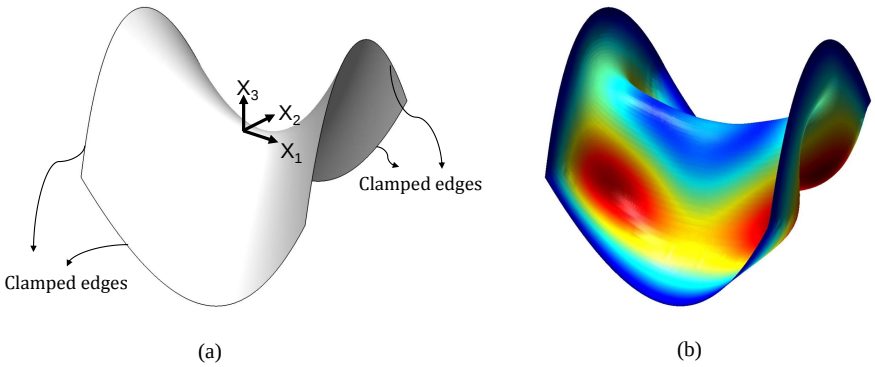

Figure 6: Un-deformed (a) and deformed configuration (b) of the thick hyperbolic paraboloid shell subjcted to pressure on the top surface. The colour contour refers to the magnitude of displacement.

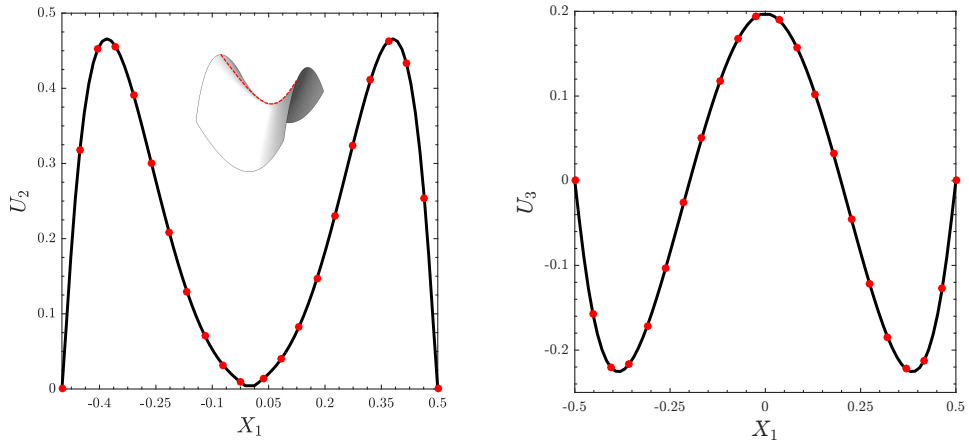

Figure 7: Displacement solution of hyperbolic paraboloid shell along X_1 with $X_2 = 0$.

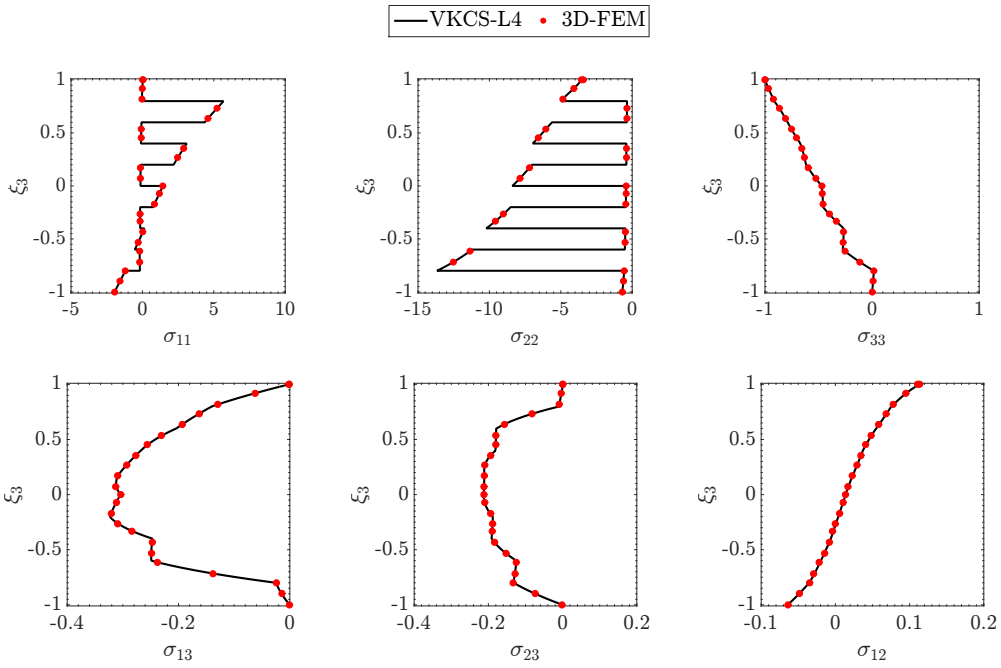

Figure 8: Through-thickness stresses at $x = -0.1, y = -0.1$ of a $(0°/90°)_5$ hypar shell subjected to uniform pressure on the top surface.

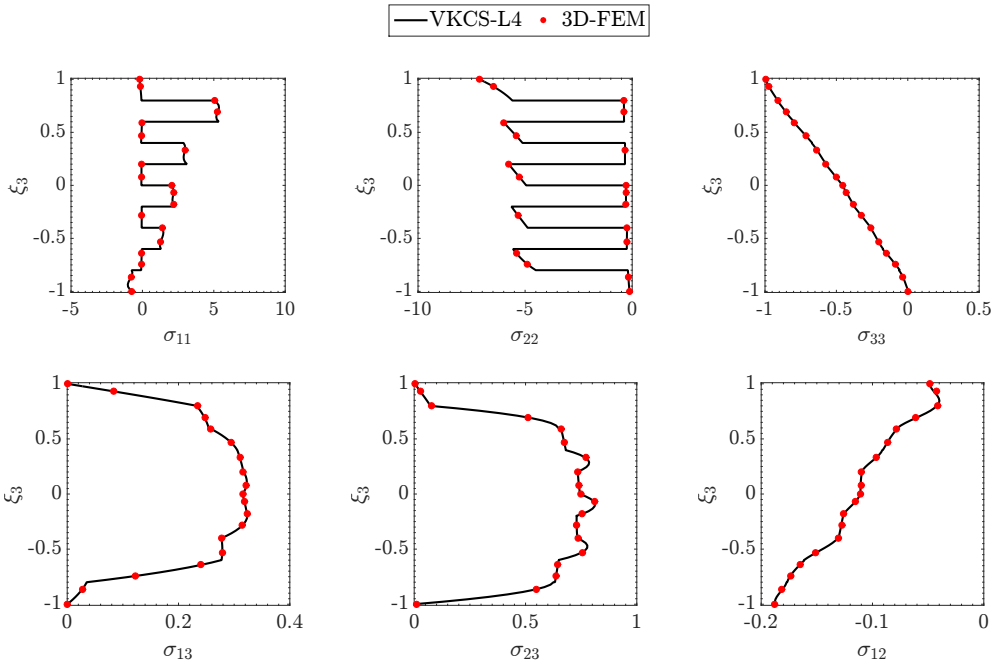

Figure 9: Through-thickness stresses at $x = -0.48, y = -0.1$ of a $(0°/90°)_5$ hypar shell subjected to uniform pressure on the top surface. The location is 2% shell planform length away from a clamped edge.

tations across the shell surface. Firstly, according to Dvorkin *et al.* [28], the material orientations can be constructed using the covariant basis vectors (as in Eq. (10)), so that the material axes always lie on the tangent planes of the three-dimensional shell geometry. The approach is convenient and does not require analytical nor additional inputs to define the material axes. However, it intrinsically couples the material orientations to the mesh configurations, hence making it difficult for material axes to be consistently defined across different meshes. As an alternative, the material axes can be analytically defined. Fig. 12 compares the material axes at the blade root using both approaches. When defined analytically, the shell normals are identical along the straight edge. On the other hand, slight deviations are observed when material axes are defined using the covariant basis vectors, as a result of the non-orthogonal local meshlines. We opted to define the material axes analytically, for the sake of consistent comparisons between models with different mesh densities and kinematic definitions.

Additionally, the definitions of the material orientations along the normals must be considered in a shell with variable thickness. The first option is keeping material orientations constant along the shell normals, as shown in Fig. 13(b). Alternatively, the material axes can vary continuously along the normals according to the local basis vectors as described by Eq. (10), shown in Fig. 13(a). We opted for the former approach because it is more consistent with the construction of a laminate with variable thickness. From a manufacturing point of view, the thickness changes in laminates are achieved by ply drops, which means that in most cases, all the plies share the same baseline material axes as the midsurface with the exception of the cover plies. The model parameters for this benchmark are shown in Table 3.

In case of a shell with variable thickness, the following transformations are carried out on

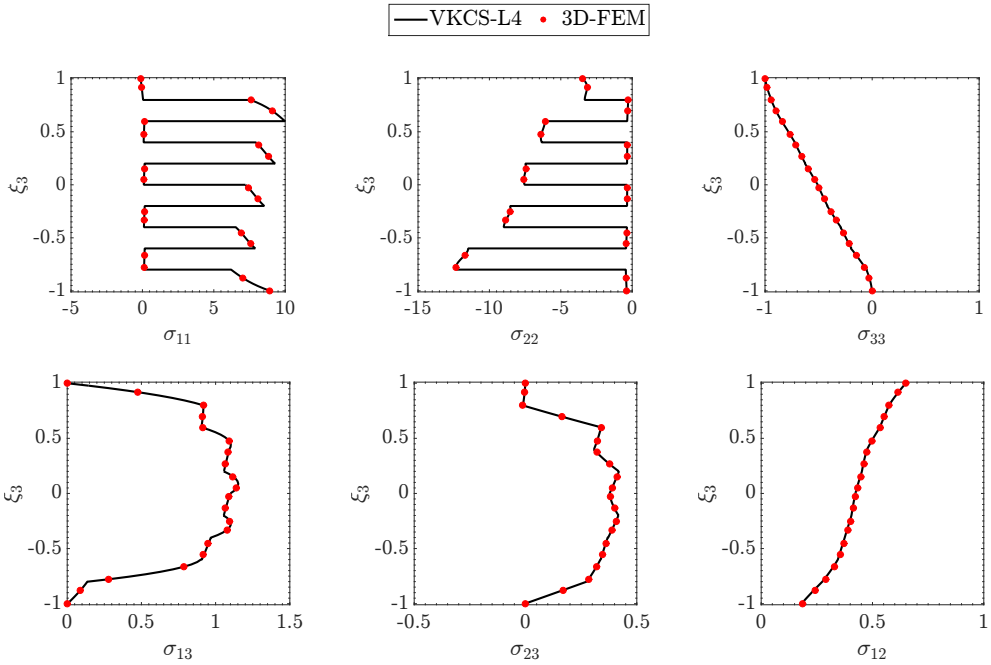

Figure 10: Through-thickness stresses at $x = -0.46, y = -0.46$ of a $(0°/90°)_5$ hypar shell subjected to uniform pressure on the top surface. The angle between the coordinate lines is greater than 40°, the location is 4% shell planform length away from a clamped edge.

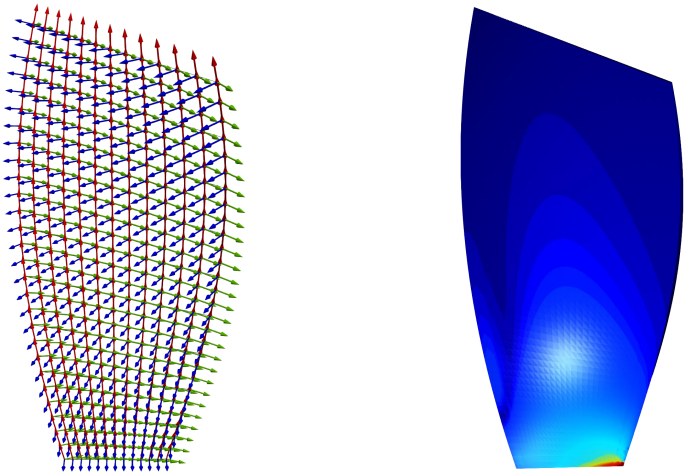

(a) (b)

Figure 11: Orientation of material axes in the in-plane domain (a) and the contour of von Mises stresses in the deformed configuration (b) of the twisted shell with variable thickness.

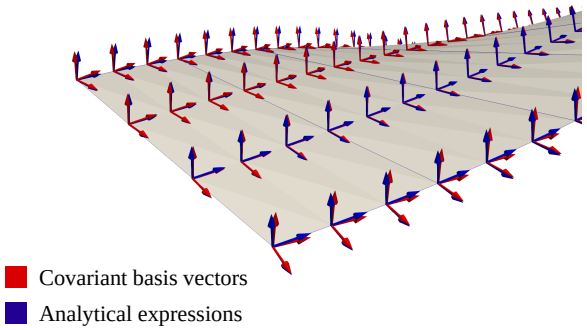

Figure 12: Comparison in the orientation of material axes in the in-plane domain as defined by the covariant basis vectors and the analytical expressions.

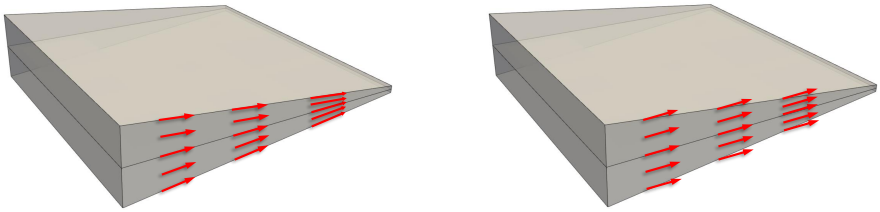

Figure 13: Two options to define the variation in fibre directions along the midplane normal: (a) fibre direction follows the tangent planes of the three-dimensional shell geometry; or (b) the material points along the midplane normal have the same fibre direction as the shell midplane.

Table 3: Model parameters for the twisted shell with variable thickness numerical benchmark.

Geometrical parameterisation

$$\mathbf{X}(r_1, r_2) = \begin{bmatrix} r_1/2 \\ (r_1+2)(r_2\cos\theta)/8 \\ (r_1+2)(-r_2\cos\theta)/8 \end{bmatrix} \text{ where } \theta = \pi(r_1+1)/6, \text{ and}$$
$$-1 \le r_1 \le 1 \text{ and } -1 \le r_2 \le 1.$$

The shell thickness distribution is

$$h(r_1, r_2) = -\tfrac{r_1}{2}(t_0 - t_1) + 0.5\,(t_0 + t_1), \text{ where } t_0 = 0.025 \text{ and } t_1 = 0.0025.$$

Material properties:

$$E_{11} = 120\times10^9,\ E_{22} = E_{33} = 10.5\times10^9,\ G_{12} = G_{23} = 5.25\times10^9,\ G_{31} = 3.48\times10^9,$$
$$\nu_{12} = \nu_{23} = 0.3 \text{ and } \nu_{13} = 0.51$$

Layup: $(45°/-45°/90°/0°)_{\text{sym}}$

Material axes:

$$\hat{\mathbf{e}}_1(r_1, r_2) = \mathbf{v}_1,$$
$$\hat{\mathbf{e}}_3(r_1, r_2) = \frac{\mathbf{v}_1 \times \mathbf{v}_2}{\|\mathbf{v}_1 \times \mathbf{v}_2\|},$$
$$\hat{\mathbf{e}}_2(r_1, r_2) = \frac{\mathbf{v}_1 \times \mathbf{v}_3}{\|\mathbf{v}_1 \times \mathbf{v}_3\|},$$

where

$$\mathbf{v}_1 = \frac{1}{2}\,\hat{\mathbf{x}}_1 + \left[\frac{v\pi}{24}\left(\frac{u}{2}+1\right)\sin\left(\frac{\pi}{6}(u+1)\right) + \frac{v}{2}\cos\left(\frac{\pi}{6}(u+1)\right)\right]\hat{\mathbf{x}}_2 + \left[\frac{-v\pi}{8}\sin\left(\frac{u+1}{6}\right)\right]\hat{\mathbf{x}}_3,$$
$$\text{and } \mathbf{v}_2 = \frac{1}{2}\,\hat{\mathbf{x}}_1 + \left(\frac{u}{4}+\frac{1}{2}\right)\cos\left(\frac{\pi(u+1)}{6}\right)\hat{\mathbf{x}}_2 + \frac{v\pi}{8}\sin\left(\frac{u+1}{6}\right)\hat{\mathbf{x}}_3.$$

Loading conditions:

Uniform pressure on the top surface $q = 1\times10^6$

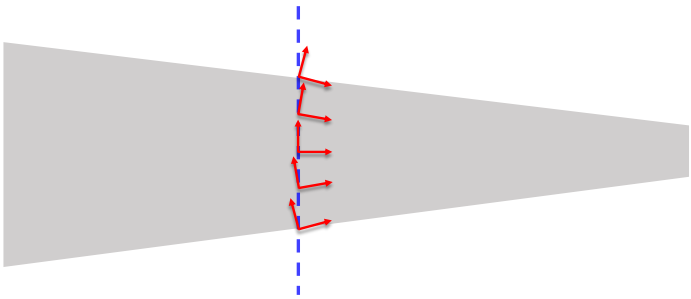

Figure 14: Cauchy stress tensors are transformed into continuously varying material axes along the shell normal.

the Cauchy stress fields. Firstly, constitutive relations are computed in the material axes on the midsurface. Then, the Cauchy stresses are computed in the local coordinate systems that lie on the tangent planes of the three-dimensional geometry. In other words, the frame of references of the Cauchy stresses change continuously along the shell normal, as shown in Fig. 14.

The implication of these transformations is that the stress tensors are no longer defined about the actual material coordinate systems. Nevertheless, this is a crucial step to approximate the traction-free conditions at the top and bottom surfaces in a variable thickness shell. In the special case of a failure analysis, the transformation step must be avoided so the Cauchy stresses correspond directly to the actual material orientations.

To demonstrate the variable-kinematics capability of the model, a parametric study is conducted across different mesh densities, and the polynomial orders of the in-plane and through-thickness displacement fields. The polynomial orders are varied from 1 to 3 for in-plane mesh densities of 5×10, 10×20 and 20×30. The reference solution is obtained from a high-fidelity 3D-FEM model in Abaqus. It is not straightforward to objectively measure the accuracy of the 3D stress solutions, as the errors may vary across different stress components and sampled locations. For simplicity, only the error of σ_{31} (often the main driver of delamination initiation) between the second and third ply from the bottom at the location $(r_1, r_2) = (-0.70, -0.70)$ is shown.

From Fig. 15, the following observations can be made: (i) none of the models with mesh 5×10 output satisfactory σ_{31} at the sampled location; (ii) for mesh 10×20, the σ_{31} solution converges to 5% of the reference solution for all models with at least cubic in-plane and quadratic through-thickness displacement fields; (iii) for mesh 20×30, the σ_{31} solution converges to 5% of the reference solution for all models with at least quadratic polynomial order in the in-plane and through-thickness domain. From an analyst's perspective, the model with 10×20 mesh with cubic in-plane and quadratic through-thickness displacement fields would be suitable for iterative design analyses, as it provides sufficiently accurate solution in σ_{31} with the lowest model size.

The observations made using Fig. 15 also suggest a threshold in through-thickness and in-plane kinematics for the convergence in σ_{31}. For the through-thickness kinematics, it is clear that at least quadratic displacement fields must be assumed, as all models across the mesh densities with linear through-thickness displacement fields output inaccurate σ_{31}. For the in-plane kinematics, models with linear displacement fields output error of $> 120\%$ from the reference solution across all mesh densities. This is because linear elements poorly represent the doubly

curved surface profiles and spatial variations of material axes.

The parametric study based on the 3D stress accuracy at a single material point must be interpreted with care. For instance, when the solution is converged for a particular *h*- level in the in-plane and through-thickness domains, the accuracy cannot be further improved via *p*- refinement in the thickness direction. The model settings circled 'A' in Fig. 15 indicate that the solution converges at quadratic through-thickness displacement field, and any further increment in the polynomial order does not improve the solution accuracy. On the contrary, the solution error can sometimes increase with the polynomial order. This is due to the oscillations in the higher-order polynomials to fit the small variations (relative to in-plane components) of through-thickness displacements. On the other hand, analysts must be mindful of outliers in the parametric map, as circled 'B' in Fig. 15. It is immediately obvious that model 'B' would not have output accurate global stresses at the particular mesh density, as indicated by the high solution error in its neighbours.

There are two competing options to enhance the in-plane kinematics, namely the mesh and polynomial order refinements of the in-plane basis functions. It is not straightforward to qualitatively determine the threshold mesh density and in-plane polynomial order for a desired level of accuracy, because the errors due to low in-plane mesh densities can always be compensated by the use of higher-order polynomial basis functions, and *vice versa*. Generally, the *p*- version of FEM has higher convergence rate in smooth elasticity problem [71, 72], which is further improved via with optimal mesh configuration (*h*- refinement). It is non-trivial to determine a combination of *hp*- settings to yield computationally efficient model at the desired level of accuracy for a specific problem. Therefore, a parametric study like Fig. 15 can aid analysts to decide the appropriate settings in the variable-kinematics framework to yield a suitable model class for their applications.

The through-thickness stresses at the locations $(r_1, r_2) = (-0.50, -0.50), (-0.70, -0.70)$ and $(-0.90, -0.75)$ are shown in Fig. 16, 17 and 18 respectively. The VKCS model has in-plane mesh density of 20×30, cubic in-plane and quadratic through-thickness displacement fields respectively, with a model size of 279 990 dofs. On the other hand, the high-fidelity 3D-FEM model consists of 1 440 000 quadratic brick elements, with model size of 18 180 099 dofs.

Across all the locations, the VKCS model shows good overall accuracy in the 3D stress field solution, where only slight discrepancies are observed for the σ_{33} component. The σ_{33} convergence of VKCS and 3D-FEM models are shown in Fig. 19, where it is clear that the 3D-FEM converges towards VKCS solution. The shell is subjected to a uniform pressure at the top surface, hence null σ_{33} is expected at the bottom surface. From Fig. 16, 17 and 18, it is clear that the solution from Abaqus does not satisfy the traction-free condition at the bottom surface. The discrepancy in the solution is because Abaqus assumes constant element-wise material axis at the element centroid, where as the material axis variation within an element is incorporated in the VKCS model. In case of a doubly-curved shell with variable-thickness, the material axes can drastically vary within an element, especially the shell normal, which has the most significant effect on the accuracy of σ_{33}.

7. Summary and future work

In this work, we derived a variable-kinematics continuum shell formulation in the framework of Carrera's Unified Formulation. The novelty is in the implementation of CUF in a continuum shell formulation. The complexity of the in-plane and through-thickness kinematics is a free parameter that can be set by the analyst. As a result, any form and order of expansion functions

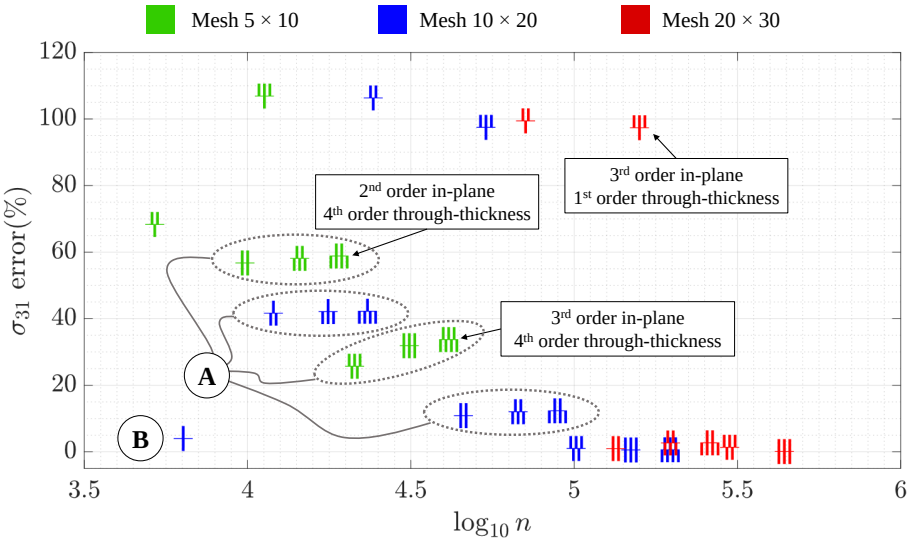

Figure 15: Parametric study showing the model accuracy in σ_{31} due to changes in model kinematics, at three different mesh densities. n is the total number of dofs. The number of top tallies indicate the order of in-plane kinematics, whereas the bottom tallies indicate the order of through-thickness kinematics. Examples of how the data points are read are shown in the figure.

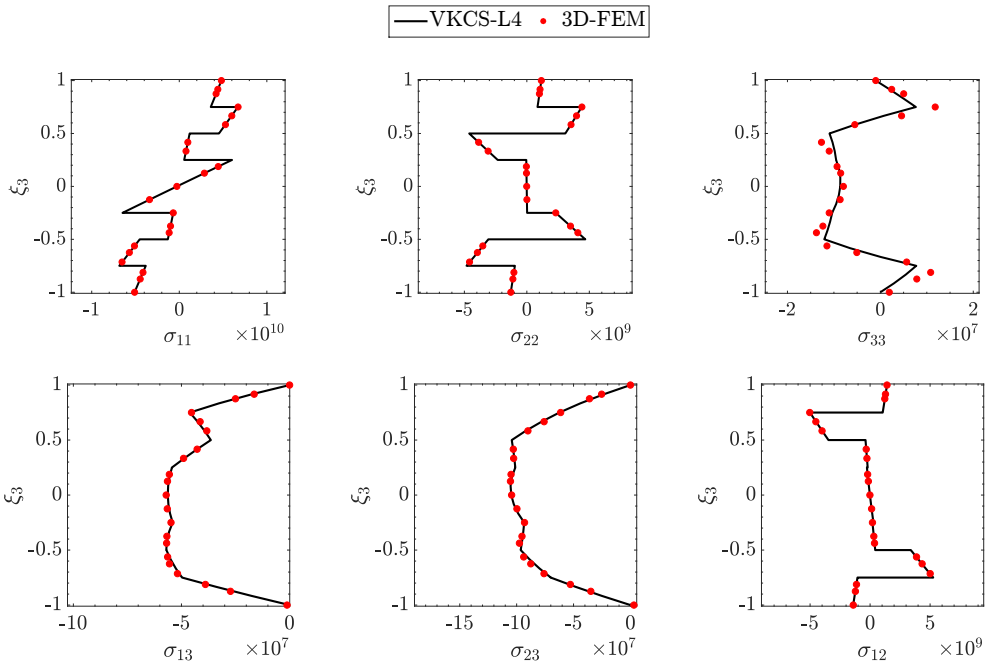

Figure 16: Through-thickness stresses at $r_1 = -0.50, r_2 = -0.50$ of a twisted laminated shell with variable thickness subjected to uniform pressure on the top surface. The local thickness is 0.01937.

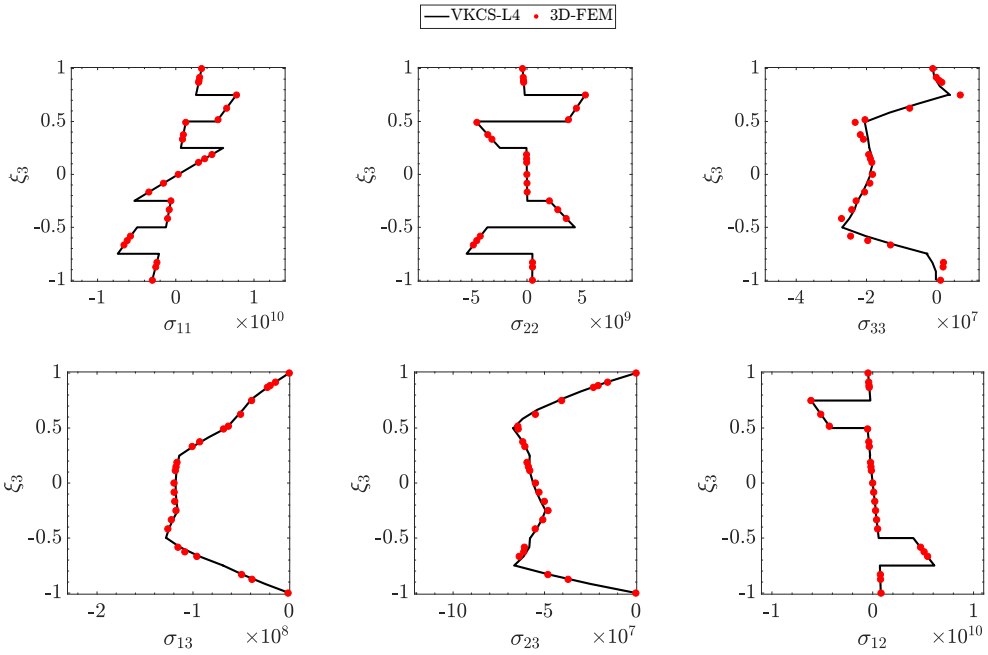

Figure 17: Through-thickness stresses at $r_1 = -0.70, r_2 = -0.70$ of a twisted laminated shell with variable thickness subjected to uniform pressure on the top surface. The local thickness is 0.02162.

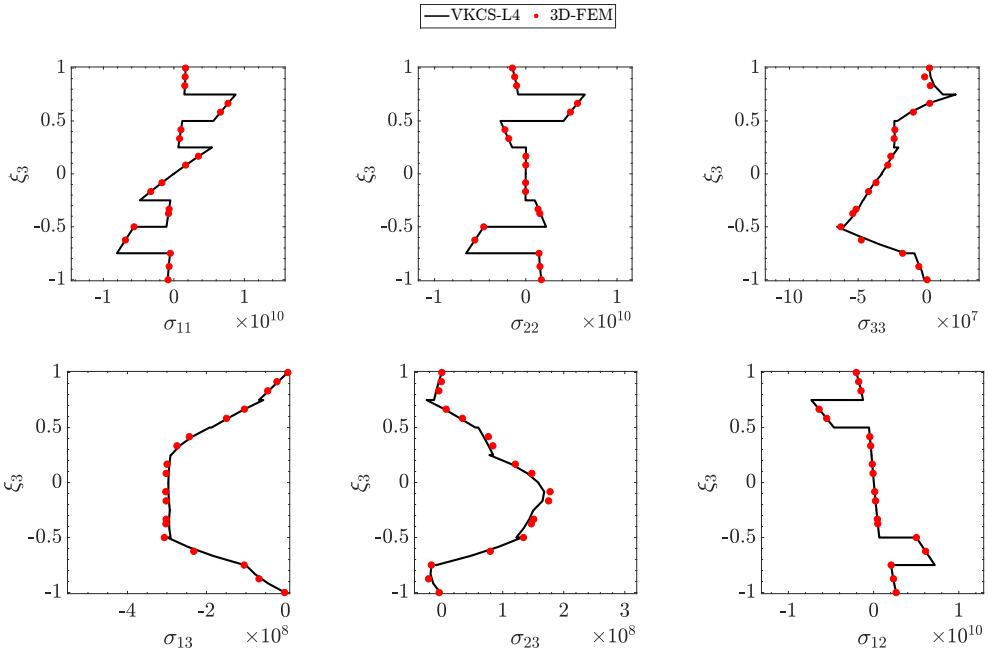

Figure 18: Through-thickness stresses at $r_1 = -0.90, r_2 = -0.75$ of a twisted laminated shell with variable thickness subjected to uniform pressure on the top surface. The local thickness is 0.02388.

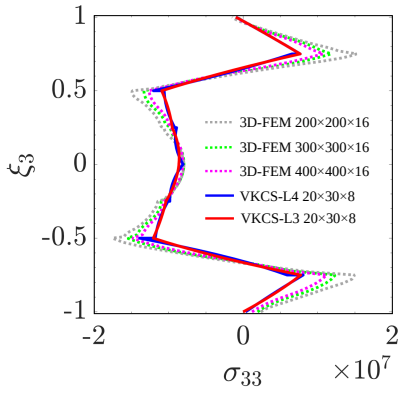

Figure 19: Convergence in σ_{33} of the VKCS and 3D-FEM models. Twenty-noded brick elements are used in the 3D-FEM solution. The in-plane mesh density is progressively increased from 200×200, 300×300 to 400×400. Each layer is modelled with two elements. The VKCS models have quadratic (L3) and cubic (L4) through-thickness displacement fields respectively. Cubic in-plane displacement fields are prescribed to both, where 20×30 elements are used in-plane, and each layer is modelled with one element.

can be prescribed without altering the pristine mesh nor the implementation code. In structural problems where appropriate model kinematics are unknown, users can gain insights into the relationships between the in-plane mesh density, model kinematics and accuracy of the specific test case by conducting a parametric study using the VKCS model. With minimal user inputs, the model settings that provide good trade-offs between computational costs and accuracy can be identified.

Two new challenging benchmarks in the analyses of laminated shells with complex geometries and highly heterogeneous layups have been proposed, namely a deep hyperbolic paraboloid shell and a twisted shell with variable thickness. The 3D stress results from the higher-order VKCS model are accurate when compared to the reference 3D solutions in all the studied benchmarks. In particular, we investigated solution accuracy in regions near the boundaries of composite structures, where stress fields are inherently three-dimensional in nature. To achieve convergence in the 3D stresses, we note that the higher-order VKCS models do not require any ad-hoc artefacts, such as shear correction factors, nor 3D stress field recovery as a post-processing step. Due to the independent *hp*- refinements in both in-plane and through-thickness domains, the model requires an order of magnitude fewer dofs and hence lower computational time, memory and storage for convergence in the stress solution. For these reasons, the VKCS element is an attractive alternative to 3D-FEM in analysing geometrically complex laminated shell structures.

In terms of wider applications, the flexibility offered by the current formulation allows model kinematics to easily be 'tuned' to suit a wide range of analyses. Therefore, analysts can bypass the need to setup multiple models for analyses requiring dissimilar levels of model fidelity. Potentially, this could inform new work flows and practices. For future work, we will include geometric nonlinearity in the current model and investigate Cauchy stresses of complex shell structures in nonlinear static and transient dynamic analyses.

8. Acknowledgement

The first author A.K.W. Hii would like to acknowledge the funding support by Rolls-Royce plc and the EPSRC through the EPSRC Centre for Doctoral Training in Advanced Composites for Innovation and Science [Grant No. EP/L016028/1]. S. Minera is supported by The H2020 Marie Skłodowska-Curie European Training Network [Grant No. R117251-101]. R.M.J. Groh is supported by the Royal Academy of Engineering under the Research Fellowship scheme [Grant No. RF/201718/17178]. A. Pirrera is supported by the EPSRC through the Early-Career Fellowship scheme [Grant No. EP/M013170/1]. L.F. Kawashita is supported by Rolls-Royce plc.

9. Bibliography

[1] J. L. Sanders Jr., "Nonlinear Theories for Thin Shells," *Quarterly of Applied Mathematics*, vol. 21, pp. 21–36, 1963.

[2] S. Ahmad, B. M. Irons, and O. C. Zienkiewicz, "Analysis of thick and thin shell structures by curved finite elements," *International Journal for Numerical Methods in Engineering*, vol. 2, no. 3, pp. 419–451, 1970.

[3] K. J. Bathe and E. N. Dvorkin, "A formulation of general shell elements—the use of mixed interpolation of tensorial components," *International Journal for Numerical Methods in Engineering*, vol. 22, no. 3, pp. 697–722, 1986.

[4] P. Yang, C. H. Norris, and Y. Stavsky, "Elastic wave propagation in heterogeneous plates," *International Journal of Solids and Structures*, vol. 2, no. 4, pp. 665–684, 1966.

[5] P. F. Pai, "A new look at shear correction factors and warping functions of anisotropic laminates," *International Journal of Solids and Structures*, vol. 32, no. 16, pp. 2295–2313, 1995.

[6] A. K. Noor, W. S. Burton, and J. M. Peters, "Predictor-corrector procedures for stress and free vibration analyses of multilayered composite plates and shells," *Computer Methods in Applied Mechanics and Engineering*, vol. 82, no. 1-3, pp. 341–363, 1990.

[7] J. M. Whitney and C. T. Sun, "A higher order theory for extensional motion of laminated composites," *Journal of Sound and Vibration*, vol. 30, no. 1, pp. 85–97, 1973.

[8] J. Reddy, "A Refined Nonlinear Theory of Plates," *International Journal of Solids and Structures*, vol. 9/10, 1983.

[9] C. W. Lim and K. M. Liew, "A higher order theory for vibration of shear deformable cylindrical shallow shells," *International Journal of Mechanical Sciences*, vol. 37, no. 3, pp. 277–295, 1995.

[10] B. Brank, J. Korelc, and A. Ibrahimbegovic, "Nonlinear shell problem formulation accounting for through-the-thickness stretching and its finite element implementation," *Computers and Structures*, vol. 80, no. 9-10, pp. 699–717, 2002.

[11] E. M. Campello, P. M. Pimenta, and P. Wriggers, "A triangular finite shell element based on a fully nonlinear shell formulation," *Computational Mechanics*, vol. 31, no. 6, pp. 505–518, 2003.

[12] N. Buchter, E. Ramm, and D. Roehl, "Three dimensional extension of nonlinear shell formulation based on the enhanced assumed strain concept," *International Journal for Numerical Methods in Engineering*, vol. 37, no. 15, pp. 2551–2568, 1994.

[13] M. Braun, M. Bischoff, and E. Ramm, "Nonlinear shell formulations for complete three-dimensional constitutive laws including composites and laminates," *Computational Mechanics*, vol. 15, no. 1, pp. 1–18, 1994.

[14] G. S. Payette and J. N. Reddy, "A seven-parameter spectral/hp finite element formulation for isotropic, laminated composite and functionally graded shell structures," *Computer Methods in Applied Mechanics and Engineering*, vol. 278, pp. 664–704, 2014.

[15] M. Gutierrez Rivera, J. N. Reddy, and M. Amabili, "A new twelve-parameter spectral/hp shell finite element for large deformation analysis of composite shells," *Composite Structures*, vol. 151, pp. 183–196, 2016.

[16] J. N. Reddy, "An evaluation of equivalent-single-layer and layerwise theories of composite laminates," *Composite Structures*, vol. 25, no. 1-4, pp. 21–35, 1993.

[17] D. H. Robbins and J. N. Reddy, "Modelling of thick composites using a layerwise laminate theory," *International Journal for Numerical Methods in Engineering*, vol. 36, no. 4, pp. 655–677, 1993.

[18] J. N. Reddy, *Theory and analysis of elastic plates and shells. Second edition*. CRC Press, 2006.

[19] E. Cosserat and F. Cosserat, "Theorie des corps deformables," *Hermann et fils (Paris)*, p. 235, 1909.

[20] W. T. Koiter, "on the Mathematical Foundation of Shell Theory," *Actes. Congres intern. Math.*, vol. 3, no. l, pp. 123–130, 1970.

[21] J. L. Sanders, "An Improved First-Approximation Theory for Thin Shells," tech. rep., National Aeronautics and Space Administration (NASA), 1959.

[22] J. Simo and D. Fox, "On a stress resultant geometrically exact shell model. Part I: Formulation and optimal parameterisation," *Computer Methods in Applied Mechanics and Engineering*, vol. 72, pp. 267–304, 1989.
[23] J. C. Simo, D. D. Fox, and M. S. Rifai, "On a stress resultant geometrically exact shell model. Part II: The linear theory; Computational aspects," *Computer Methods in Applied Mechanics and Engineering*, vol. 73, no. 1, pp. 53–92, 1989.
[24] J. Simo, D. Fox, and M. Rifai, "On a stress resultant geometrically exact shell model. Part III: The linear theory; Computational aspects," *Computer Methods in Applied Mechanics and Engineering*, vol. 73, no. 1, pp. 53–92, 1989.
[25] J. C. Simo, M. S. Rifai, and D. D. Fox, "On a stress resultant geometrically exact shell model. Part IV: Variable thickness shells with through-the-thickness stretching," *Computer Methods in Applied Mechanics and Engineering*, vol. 81, no. 1, pp. 91–126, 1990.
[26] T. J. Hughes and W. K. Liu, "Nonlinear finite element analysis of shells: Part I. three-dimensional shells," *Computer Methods in Applied Mechanics and Engineering*, vol. 26, no. 3, pp. 331–362, 1981.
[27] T. J. Hughes and W. K. Liu, "Nonlinear finite element analysis of shells-part II. two-dimensional shells," *Computer Methods in Applied Mechanics and Engineering*, vol. 27, no. 2, pp. 167–181, 1981.
[28] E. N. Dvorkin and K.-J. Bathe, "A Continuum Mechanics based four-node element for general non-linear analysis," *Engineering Computations*, vol. 1, no. 1, pp. 77–88, 1984.
[29] W. K. Liu, E. S. Law, D. Lam, and T. Belytschko, "Resultant-stress degenerated-shell element," *Computer Methods in Applied Mechanics and Engineering*, vol. 55, no. 3, pp. 259–300, 1986.
[30] N. Büchter and E. Ramm, "Shell theory versus degeneration - a comparison in large rotation finite element analysis," *International Journal for Numerical Methods in Engineering*, vol. 34, no. December 1990, pp. 39–59, 1992.
[31] H. T. Y. Yang, S. Saigal, A. Masud, and R. K. Kapania, "A survey of recent shell finite elements," *International Journal for Numerical Methods in Engineering*, vol. 47, no. 1-3, pp. 101–127, 2000.
[32] J. N. Reddy and R. A. Arciniega, "Shear deformation plate and shell theories: From Stavsky to present," *Mechanics of Advanced Materials and Structures*, vol. 11, no. 6 II, pp. 535–582, 2004.
[33] A. Düster, H. Br Ker, and E. Rank, "The p-version of the finite element method for three-dimensional curved thin walled structures," *International Journal for Numerical Methods in Engineering*, vol. 52, no. 7, pp. 673–703, 2001.
[34] R. L. Actis and B. A. Szabó, "Hierarchic Models for Plates and Shells," *Computer Methods in Applied Mechanics and Engineering*, pp. 129–133, 1997.
[35] T. O. Williams, "A generalized multilength scale nonlinear composite plate theory with delamination," *International Journal of Solids and Structures*, vol. 36, no. 20, pp. 3015–3050, 1999.
[36] T. O. Williams, "A new theoretical framework for the formulation of general, nonlinear, multiscale plate theories," *International Journal of Solids and Structures*, vol. 45, no. 9, pp. 2534–2560, 2008.
[37] T. O. Williams, "A new, unified, theoretical framework for the formulation of general, nonlinear, single-scale shell theories," *Composite Structures*, vol. 107, pp. 544–558, 2014.
[38] E. Carrera and L. Demasi, "Classical and advanced multilayered plate elements based upon PVD and RMVT. Part 2: Numerical implementations," *International Journal for Numerical Methods in Engineering*, vol. 55, no. 3, pp. 253–291, 2002.
[39] L. Demasi, "Inf Hierarchy plate theories for thick and thin composite plates: The generalized unified formulation," *Composite Structures*, vol. 84, no. 3, pp. 256–270, 2008.
[40] A. Entezari, M. A. Kouchakzadeh, E. Carrera, and M. Filippi, "A refined finite element method for stress analysis of rotors and rotating disks with variable thickness," *Acta Mechanica*, vol. 228, no. 2, pp. 575–594, 2017.
[41] S. Minera, M. Patni, E. Carrera, M. Petrolo, P. M. Weaver, and A. Pirrera, "Three-dimensional stress analysis for beam-like structures using Serendipity Lagrange shape functions," *International Journal of Solids and Structures*, vol. 0, pp. 1–18, 2018.
[42] A. J. M. Ferreira, C. M. C. Roque, E. Carrera, and M. Cinefra, "Analysis of thick isotropic and cross-ply laminated plates by radial basis functions and a Unified Formulation," *Journal of Sound and Vibration*, vol. 330, no. 4, pp. 771–787, 2011.
[43] S. Natarajan, A. Ferreira, and H. Nguyen-Xuan, "Analysis of cross-ply laminated plates using isogeometric analysis and unified formulation," *Curved and Layer. Struct.*, vol. 1, pp. 1–10, 2014.
[44] M. Cinefra and S. Valvano, "A variable kinematic doubly-curved MITC9 shell element for the analysis of laminated composites," *Mechanics of Advanced Materials and Structures*, vol. 23, no. 11, pp. 1312–1325, 2016.
[45] F. Tornabene, "General higher-order layer-wise theory for free vibrations of doubly-curved laminated composite shells and panels," *Mechanics of Advanced Materials and Structures*, vol. 23, no. 9, pp. 1046–1067, 2016.
[46] F. Tornabene, N. Fantuzzi, and M. Bacciocchi, "The local GDQ method applied to general higher-order theories of doubly-curved laminated composite shells and panels: The free vibration analysis," *Composite Structures*, vol. 116, no. 1, pp. 637–660, 2014.
[47] F. Tornabene, N. Fantuzzi, M. Bacciocchi, and E. Viola, "A new approach for treating concentrated loads in doubly-curved composite deep shells with variable radii of curvature," *Composite Structures*, vol. 131, pp. 433–452, 2015.

[48] F. Tornabene, N. Fantuzzi, and M. Bacciocchi, "The local GDQ method for the natural frequencies of doubly-curved shells with variable thickness: A general formulation," *Composites Part B: Engineering*, vol. 92, pp. 265–289, 2016.
[49] M. Bacciocchi, M. Eisenberger, N. Fantuzzi, F. Tornabene, and E. Viola, "Vibration analysis of variable thickness plates and shells by the Generalized Differential Quadrature method," *Composite Structures*, vol. 156, pp. 218–237, 2016.
[50] A. Pirrera and P. M. Weaver, "Geometrically Nonlinear First-Order Shear Deformation Theory for General Anisotropic Shells," *AIAA Journal*, vol. 47, no. 3, pp. 767–782, 2009.
[51] I. Sokolnikoff, *Mathematical theory of elasticity*. New York: McGraw-Hill, 1956.
[52] S. T. Dennis and A. N. Palazotto, *Nonlinear Analysis of Shell Structures*. American Institute of Aeronautics and Astronautics, 1992.
[53] M. P. Nemeth, "An Exposition on the Nonlinear Kinematics of Shells , Including Transverse Shearing Deformations," Tech. Rep. February, Langley Research Center, Hampton, Virginia, 2013.
[54] E. Abbena, S. Salamon, and A. Gray, *Modern Differential Geometry of Curves and Surfaces with Mathematica*. CRC Press, third ed., 2017.
[55] M. Bischoff, W. Wall, K. Bletzinger, and E. Ramm, "Models and Finite Elements for Thin-walled Structures," *Encyclopedia of Computational Mechanics*, no. 1859, 2004.
[56] O. C. Zienkiewicz and R. L. Taylor, *The Finite Element Method Volume 1 : The Basis*, vol. 1. Butterworth-Heinemann, fifth ed., 2000.
[57] O. C. Zienkiewicz and R. Taylor, *The Finite Element Method Volume 2 : Solid and structural mechanics*. Butterworth-Heinemann, seventh ed., 2014.
[58] K. J. Bathe and A. P. Cimento, "Some practical procedures for the solution of nonlinear finite element equations," *Computer Methods in Applied Mechanics and Engineering*, vol. 22, no. 1, pp. 59–85, 1980.
[59] P. Wriggers, R. Eberlein, and S. Reese, "A comparison of three-dimensional continuum and shell elements for finite plasticity," *International Journal of Solids and Structures*, vol. 33, no. 20, pp. 3309–3326, 1996.
[60] K. Bathe, *Finite element procedures. Second edition*. Prentice Hall, 2006.
[61] E. Carrera, M. Cinefra, M. Petrolo, and E. Zappino, *Finite element analysis of structures through unified formulation*. John Wiley & Sons, 2014.
[62] M. Cinefra, E. Carrera, and S. Valvano, "Variable kinematic shell elements for the analysis of electro-mechanical Problems," *Mechanics of Advanced Materials and Structures*, vol. 22, no. 1-2, pp. 77–106, 2015.
[63] L. Demasi, "Inf6 Mixed plate theories based on the Generalized Unified Formulation. Part IV: Zig-zag theories," *Composite Structures*, vol. 87, no. 3, pp. 195–205, 2009.
[64] M. Cinefra, M. Petrolo, G. Li, and E. Carrera, "Variable kinematic shell elements for composite laminates accounting for hygrothermal effects," *Journal of Thermal Stresses*, vol. 40, no. 12, pp. 1523–1544, 2017.
[65] H. S. Kim, A. Chattopadhyay, and A. Ghoshal, "Characterization of delamination effect on composite laminates using a new generalized layerwise approach," *Computers and Structures*, vol. 81, no. 15, pp. 1555–1566, 2003.
[66] E. Carrera, S. Brischetto, and P. Nali, "Variational statements and computational models for multifield problems and multilayered structures," *Mechanics of Advanced Materials and Structures*, vol. 15, no. 3-4, pp. 182–198, 2008.
[67] K. Bhaskar and T. K. Varadan, "Exact Elasticity Solution for Laminated Anisotropic Cylindrical Shells," *Journal of Applied Mechanics*, vol. 60, no. 1, pp. 41–47, 1993.
[68] M. Omurtag and A. Aköz, "Hyperbolic paraboloid shell analysis via mixed finite element formulation," *International Journal for Numerical Methods in Engineering*, vol. 37, no. 18, pp. 3037–3056, 1994.
[69] P. Gergely and P. V. Banavalkar, "The analysis and behavior of thin-steel hyperbolic paraboloid shells," *Center for Cold-Formed Steel Structures Library*, 1971.
[70] J. Chróścielewski, I. Kreja, A. Sabik, and W. Witkowski, "Modeling of composite shells in 6-parameter nonlinear theory with drilling degree of freedom," *Mechanics of Advanced Materials and Structures*, vol. 18, no. 6, pp. 403–419, 2011.
[71] I. Babuska, A. Szabo, and I. Katz, "The p-version of the Finite Element Method," *SIAM journal on Numerical Analysis*, vol. 18, no. 3, pp. 515–545, 1981.
[72] I. Babuka and M. Suri, "The Optimal Convergence Rate of the p-Version of the Finite Element Method Author," *SIAM journal on Numerical Analysis*, vol. 24, no. 4, pp. 750–776, 1987.

Appendix A. Explicit expressions of *Fundamental Nuclei* of VKCS

We present the explicit expressions for the *Fundamental Nuclei* of the VKCS formulation. The factorisation scheme below has been defined to simplify the analytical expressions:

$$
\begin{aligned}
D_1 &= F_s \frac{\partial N_j}{\partial \xi_1} \\
D_2 &= F_s \frac{\partial N_j}{\partial \xi_2} \\
D_3 &= \frac{\partial F_s}{\partial \xi_3} N_j
\end{aligned}
\tag{A.1}
$$

$$
\begin{aligned}
E_1 &= F_\tau \frac{\partial N_i}{\partial \xi_1} \\
E_2 &= F_\tau \frac{\partial N_i}{\partial \xi_2} \\
E_3 &= \frac{\partial F_\tau}{\partial \xi_3} N_i
\end{aligned}
\tag{A.2}
$$

$$
\begin{aligned}
B_1 &= D_2 \frac{\partial X_1}{\partial \xi_1} + D_1 \frac{\partial X_1}{\partial \xi_2} \\
B_2 &= D_3 \frac{\partial X_1}{\partial \xi_1} + D_1 \frac{\partial X_1}{\partial \xi_3} \\
B_3 &= D_3 \frac{\partial X_1}{\partial \xi_2} + D_2 \frac{\partial X_1}{\partial \xi_3} \\
B_4 &= D_2 \frac{\partial X_2}{\partial \xi_1} + D_1 \frac{\partial X_2}{\partial \xi_2} \\
B_5 &= D_3 \frac{\partial X_2}{\partial \xi_1} + D_1 \frac{\partial X_2}{\partial \xi_3} \\
B_6 &= D_3 \frac{\partial X_2}{\partial \xi_2} + D_2 \frac{\partial X_2}{\partial \xi_3} \\
B_7 &= D_2 \frac{\partial X_3}{\partial \xi_1} + D_1 \frac{\partial X_3}{\partial \xi_2} \\
B_8 &= D_3 \frac{\partial X_3}{\partial \xi_1} + D_1 \frac{\partial X_3}{\partial \xi_3} \\
B_9 &= D_3 \frac{\partial X_3}{\partial \xi_2} + D_2 \frac{\partial X_3}{\partial \xi_3}
\end{aligned}
\tag{A.3}
$$

$$
\begin{aligned}
A_1 &= C^{1111} D_1 \frac{\partial X_1}{\partial \xi_1} + C^{1122} D_2 \frac{\partial X_1}{\partial \xi_2} + C^{1112} B_1 + C^{1133} D_3 \frac{\partial X_1}{\partial \xi_3} + C^{1113} B_2 + C^{1123} B_3 \\
A_2 &= C^{1122} D_1 \frac{\partial X_1}{\partial \xi_1} + C^{2222} D_2 \frac{\partial X_1}{\partial \xi_2} + C^{2212} B_1 + C^{2233} D_3 \frac{\partial X_1}{\partial \xi_3} + C^{2213} B_2 + C^{2223} B_3 \\
A_3 &= C^{1133} D_1 \frac{\partial X_1}{\partial \xi_1} + C^{2233} D_2 \frac{\partial X_1}{\partial \xi_2} + C^{3312} B_1 + C^{3333} D_3 \frac{\partial X_1}{\partial \xi_3} + C^{3313} B_2 + C^{3323} B_3 \\
A_4 &= C^{1123} D_1 \frac{\partial X_1}{\partial \xi_1} + C^{2223} D_2 \frac{\partial X_1}{\partial \xi_2} + C^{2312} B_1 + C^{3323} D_3 \frac{\partial X_1}{\partial \xi_3} + C^{2313} B_2 + C^{2323} B_3
\end{aligned}
$$

$$
\begin{aligned}
A_5 &= C^{1113}D_1\frac{\partial X_1}{\partial \xi_1} + C^{2213}D_2\frac{\partial X_1}{\partial \xi_2} + C^{1312}B_1 + C^{3313}D_3\frac{\partial X_1}{\partial \xi_3} + C^{1313}B_2 + C^{2313}B_3 \\
A_6 &= C^{1112}D_1\frac{\partial X_1}{\partial \xi_1} + C^{2212}D_2\frac{\partial X_1}{\partial \xi_2} + C^{1212}B_1 + C^{3312}D_3\frac{\partial X_1}{\partial \xi_3} + C^{1312}B_2 + C^{2312}B_3 \\
A_7 &= C^{1111}D_1\frac{\partial X_2}{\partial \xi_1} + C^{1122}D_2\frac{\partial X_2}{\partial \xi_2} + C^{1112}B_4 + C^{1133}D_3\frac{\partial X_2}{\partial \xi_3} + C^{1113}B_5 + C^{1123}B_6 \\
A_8 &= C^{1122}D_1\frac{\partial X_2}{\partial \xi_1} + C^{2222}D_2\frac{\partial X_2}{\partial \xi_2} + C^{2212}B_4 + C^{2233}D_3\frac{\partial X_2}{\partial \xi_3} + C^{2213}B_5 + C^{2223}B_6 \\
A_9 &= C^{1133}D_1\frac{\partial X_2}{\partial \xi_1} + C^{2233}D_2\frac{\partial X_2}{\partial \xi_2} + C^{3312}B_4 + C^{3333}D_3\frac{\partial X_2}{\partial \xi_3} + C^{3313}B_5 + C^{3323}B_6 \\
A_{10} &= C^{1123}D_1\frac{\partial X_2}{\partial \xi_1} + C^{2223}D_2\frac{\partial X_2}{\partial \xi_2} + C^{2312}B_4 + C^{3323}D_3\frac{\partial X_2}{\partial \xi_3} + C^{2313}B_5 + C^{2323}B_6 \\
A_{11} &= C^{1113}D_1\frac{\partial X_2}{\partial \xi_1} + C^{2213}D_2\frac{\partial X_2}{\partial \xi_2} + C^{1312}B_4 + C^{3313}D_3\frac{\partial X_2}{\partial \xi_3} + C^{1313}B_5 + C^{2313}B_6 \\
A_{12} &= C^{1112}D_1\frac{\partial X_2}{\partial \xi_1} + C^{2212}D_2\frac{\partial X_2}{\partial \xi_2} + C^{1212}B_4 + C^{3312}D_3\frac{\partial X_2}{\partial \xi_3} + C^{1312}B_5 + C^{2312}B_6 \\
A_{13} &= C^{1111}D_1\frac{\partial X_3}{\partial \xi_1} + C^{1122}D_2\frac{\partial X_3}{\partial \xi_2} + C^{1112}B_7 + C^{1133}D_3\frac{\partial X_3}{\partial \xi_3} + C^{1113}B_8 + C^{1123}B_9 \\
A_{14} &= C^{1122}D_1\frac{\partial X_3}{\partial \xi_1} + C^{2222}D_2\frac{\partial X_3}{\partial \xi_2} + C^{2212}B_7 + C^{2233}D_3\frac{\partial X_3}{\partial \xi_3} + C^{2213}B_8 + C^{2223}B_9 \\
A_{15} &= C^{1133}D_1\frac{\partial X_3}{\partial \xi_1} + C^{2233}D_2\frac{\partial X_3}{\partial \xi_2} + C^{3312}B_7 + C^{3333}D_3\frac{\partial X_3}{\partial \xi_3} + C^{3313}B_8 + C^{3323}B_9 \\
A_{16} &= C^{1123}D_1\frac{\partial X_3}{\partial \xi_1} + C^{2223}D_2\frac{\partial X_3}{\partial \xi_2} + C^{2312}B_7 + C^{3323}D_3\frac{\partial X_3}{\partial \xi_3} + C^{2313}B_8 + C^{2323}B_9 \\
A_{17} &= C^{1113}D_1\frac{\partial X_3}{\partial \xi_1} + C^{2213}D_2\frac{\partial X_3}{\partial \xi_2} + C^{1312}B_7 + C^{3313}D_3\frac{\partial X_3}{\partial \xi_3} + C^{1313}B_8 + C^{2313}B_9 \\
A_{18} &= C^{1112}D_1\frac{\partial X_3}{\partial \xi_1} + C^{2212}D_2\frac{\partial X_3}{\partial \xi_2} + C^{1212}B_7 + C^{3312}D_3\frac{\partial X_3}{\partial \xi_3} + C^{1312}B_8 + C^{2312}B_9.
\end{aligned}
\tag{A.4}
$$

We write the nine components of $\mathbf{k}^{(e)}_{ij\tau s}$ as follows, note that the $ij\tau s$ are superscripted to allow for the indexing of the coefficients in the *Fundamental Nuclei*:

$$
\mathbf{k}^{(e)}_{ij\tau s} = \begin{bmatrix} k^{ij\tau s}_{11} & k^{ij\tau s}_{12} & k^{ij\tau s}_{13} \\ k^{ij\tau s}_{21} & k^{ij\tau s}_{22} & k^{ij\tau s}_{23} \\ k^{ij\tau s}_{31} & k^{ij\tau s}_{32} & k^{ij\tau s}_{33} \end{bmatrix}
\tag{A.5}
$$

$$
\begin{aligned}
k^{ij\tau s}_{11} = \int & E_1\frac{\partial X_1}{\partial \xi_1}A_1 + E_2\frac{\partial X_1}{\partial \xi_2}A_2 + E_3\frac{\partial X_1}{\partial \xi_3}A_3 + (E_3\frac{\partial X_1}{\partial \xi_2} + E_2\frac{\partial X_1}{\partial \xi_3})A_4 + \\
& (E_3\frac{\partial X_1}{\partial \xi_1} + E_1\frac{\partial X_1}{\partial \xi_3})A_5 + (E_2\frac{\partial X_1}{\partial \xi_1} + E_1\frac{\partial X_1}{\partial \xi_2})A_6 \; d\mathcal{B}
\end{aligned}
\tag{A.6}
$$

$$k_{12}^{ij\tau s} = \int E_1 A_1 \frac{\partial X_2}{\partial \xi_1} + E_2 A_2 \frac{\partial X_2}{\partial \xi_2} + A_6(E_2 \frac{\partial X_2}{\partial \xi_1} + E_1 \frac{\partial X_2}{\partial \xi_2}) + E_3 A_3 \frac{\partial X_2}{\partial \xi_3} + A_5(E_3 \frac{\partial X_2}{\partial \xi_1} + E_1 \frac{\partial X_2}{\partial \xi_3}) + A_4(E_3 \frac{\partial X_2}{\partial \xi_2} + E_2 \frac{\partial X_2}{\partial \xi_3})\ d\mathcal{B} \tag{A.7}$$

$$k_{13}^{ij\tau s} = \int E_1 A_1 \frac{\partial X_3}{\partial \xi_1} + E_2 A_2 \frac{\partial X_3}{\partial \xi_2} + A_6(E_2 \frac{\partial X_3}{\partial \xi_1} + E_1 \frac{\partial X_3}{\partial \xi_2}) + E_3 A_3 \frac{\partial X_3}{\partial \xi_3} + A_5(E_3 \frac{\partial X_3}{\partial \xi_1} + E_1 \frac{\partial X_3}{\partial \xi_3}) + A_4(E_3 \frac{\partial X_3}{\partial \xi_2} + E_2 \frac{\partial X_3}{\partial \xi_3})\ d\mathcal{B} \tag{A.8}$$

$$k_{21}^{ij\tau s} = \int E_1 \frac{\partial X_1}{\partial \xi_1} A_7 + E_2 \frac{\partial X_1}{\partial \xi_2} A_8 + E_3 \frac{\partial X_1}{\partial \xi_3} A_9 + (E_3 \frac{\partial X_1}{\partial \xi_2} + E_2 \frac{\partial X_1}{\partial \xi_3}) A_{10} + (E_3 \frac{\partial X_1}{\partial \xi_1} + E_1 \frac{\partial X_1}{\partial \xi_3}) A_{11} + (E_2 \frac{\partial X_1}{\partial \xi_1} + E_1 \frac{\partial X_1}{\partial \xi_2}) A_{12}\ d\mathcal{B} \tag{A.9}$$

$$k_{22}^{ij\tau s} = \int E_1 \frac{\partial X_2}{\partial \xi_1} A_7 + E_2 \frac{\partial X_2}{\partial \xi_2} A_8 + E_3 \frac{\partial X_2}{\partial \xi_3} A_9 + (E_3 \frac{\partial X_2}{\partial \xi_2} + E_2 \frac{\partial X_2}{\partial \xi_3}) A_{10} + (E_3 \frac{\partial X_2}{\partial \xi_1} + E_1 \frac{\partial X_2}{\partial \xi_3}) A_{11} + (E_2 \frac{\partial X_2}{\partial \xi_1} + E_1 \frac{\partial X_2}{\partial \xi_2}) A_{12}\ d\mathcal{B} \tag{A.10}$$

$$k_{23}^{ij\tau s} = \int E_1 A_7 \frac{\partial X_3}{\partial \xi_1} + E_2 A_8 \frac{\partial X_3}{\partial \xi_2} + A_{12}(E_2 \frac{\partial X_3}{\partial \xi_1} + E_1 \frac{\partial X_3}{\partial \xi_2}) + E_3 A_9 \frac{\partial X_3}{\partial \xi_3} + A_{11}(E_3 \frac{\partial X_3}{\partial \xi_1} + E_1 \frac{\partial X_3}{\partial \xi_3}) + A_{10}(E_3 \frac{\partial X_3}{\partial \xi_2} + E_2 \frac{\partial X_3}{\partial \xi_3})\ d\mathcal{B} \tag{A.11}$$

$$k_{31}^{ij\tau s} = \int E_1 \frac{\partial X_1}{\partial \xi_1} A_{13} + E_2 \frac{\partial X_1}{\partial \xi_2} A_{14} + E_3 \frac{\partial X_1}{\partial \xi_3} A_{15} + (E_3 \frac{\partial X_1}{\partial \xi_2} + E_2 \frac{\partial X_1}{\partial \xi_3}) A_{16} + (E_3 \frac{\partial X_1}{\partial \xi_1} + E_1 \frac{\partial X_1}{\partial \xi_3}) A_{17} + (E_2 \frac{\partial X_1}{\partial \xi_1} + E_1 \frac{\partial X_1}{\partial \xi_2}) A_{18}\ d\mathcal{B} \tag{A.12}$$

$$k_{32}^{ij\tau s} = \int E_1 \frac{\partial X_2}{\partial \xi_1} A_{13} + E_2 \frac{\partial X_2}{\partial \xi_2} A_{14} + E_3 \frac{\partial X_2}{\partial \xi_3} A_{15} + (E_3 \frac{\partial X_2}{\partial \xi_2} + E_2 \frac{\partial X_2}{\partial \xi_3}) A_{16} + (E_3 \frac{\partial X_2}{\partial \xi_1} + E_1 \frac{\partial X_2}{\partial \xi_3}) A_{17} + (E_2 \frac{\partial X_2}{\partial \xi_1} + E_1 \frac{\partial X_2}{\partial \xi_2}) A_{18}\ d\mathcal{B} \tag{A.13}$$

$$k_{33}^{ij\tau s} = \int E_1 \frac{\partial X_3}{\partial \xi_1} A_{13} + E_2 \frac{\partial X_3}{\partial \xi_2} A_{14} + E_3 \frac{\partial X_3}{\partial \xi_3} A_{15} + (E_3 \frac{\partial X_3}{\partial \xi_2} + E_2 \frac{\partial X_3}{\partial \xi_3}) A_{16} + (E_3 \frac{\partial X_3}{\partial \xi_1} + E_1 \frac{\partial X_3}{\partial \xi_3}) A_{17} + (E_2 \frac{\partial X_3}{\partial \xi_1} + E_1 \frac{\partial X_3}{\partial \xi_2}) A_{18}\ d\mathcal{B}. \tag{A.14}$$